Cell Reports
Medicine

Article

Ribosome dysregulation and intervention in age-related infertility

Graphical abstract

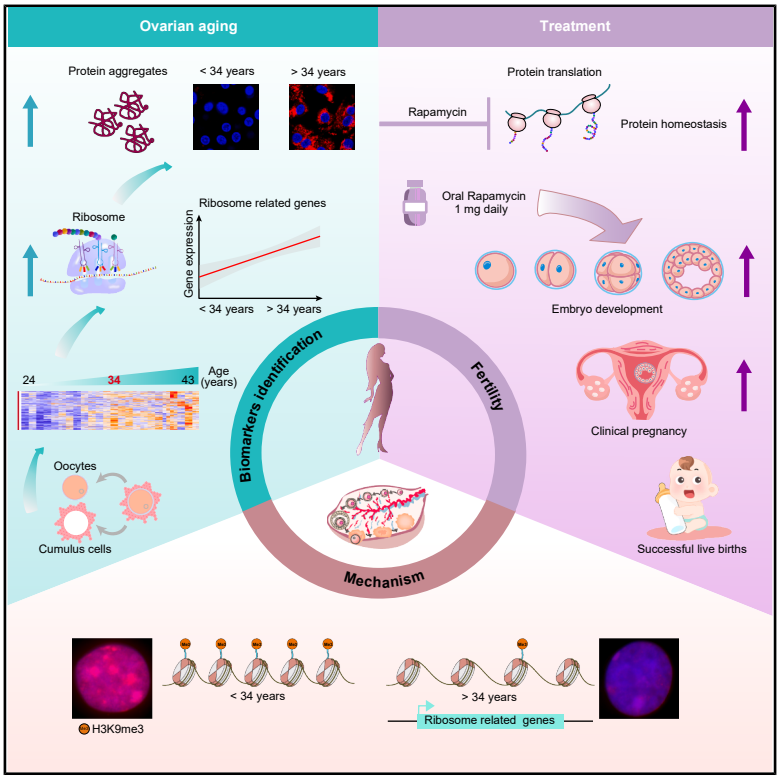

Highlights

- Oocytes and cumulus cells exhibit striking transcriptional changes by the age of 34
- Multi-omics identifies ribosome dysregulation as a new biomarker of ovarian aging
- Reduced H3K9me3 abundance is linked to upregulation of ribosome genes with age
- Short-term rapamycin treatment improves embryo quality, pregnancy, and live births

Authors

Jie Li, Honghong Wang, Pengfei Zhu, ..., Wei Shang, Xueqing Wu, Lin Liu

Correspondence

bxhjj@163.com (X.B.),
shang.wei@163.com (W.S.),
wuxueqq@hotmail.com (X.W.),
liulin@nankai.edu.cn (L.L.)

In brief

In this paper, Li et al. reveal that ribosome dysregulation in oocytes and cumulus cells contributes to age-related infertility and demonstrate that rapamycin treatment can improve pregnancy outcomes in women by restoring protein homeostasis.

Li et al., 2025, Cell Reports Medicine 6, 102424
November 18, 2025
https://doi.org/10.1016/j.xcrm.2025.102424

CellPress

Cell Reports Medicine

CellPress
OPEN ACCESS

Article

Ribosome dysregulation and intervention in age-related infertility

Jie Li,[1,2,12] Honghong Wang,[3,4,12] Pengfei Zhu,[3,4,12] Haixia Chen,[5,12] Haiyang Zuo,[6,12] Chang Liu,[1,2,12] Linlin Liu,[1,2] Xiaoying Ye,[1,2] Guofeng Feng,[1,2] Yiwei Wu,[1,2] Qinli Liu,[7] Tao Yang,[8,9] David L. Keefe,[10] Xiaohong Bai,[5,*] Wei Shang,[6,*] Xueqing Wu,[3,4,*] and Lin Liu[1,2,11,13,*]

[1]State Key Laboratory of Medicinal Chemical Biology, Nankai University, Tianjin 300350, China
[2]Department of Cell Biology and Genetics, Nankai University, 94 Weijin Road, Tianjin 300071, China
[3]Center for Reproductive Medicine, Children's Hospital of Shanxi and Women Health Center of Shanxi, Taiyuan 030013, China
[4]Shanxi Center of Technology Innovation for Fertility Optimization, Taiyuan 030001, Shanxi, China
[5]Center for Reproductive Medicine, Tianjin Medical University General Hospital, Tianjin 300052, China
[6]Department of Obstetrics and Gynecology, The Sixth Medical Center of Chinese People's Liberation Army (PLA) General Hospital, Beijing 100142, China
[7]Reproductive Medical Center, Amcare Women's & Children's Hospital, Tianjin 300381, China
[8]Higher Education Key Laboratory of Tumor Immunology & Targeted Drug Development in Shanxi Province, Shanxi Medical University, Taiyuan 030001, Shanxi, China
[9]Department of Biochemistry & Molecular Biology, Shanxi Medical University, Taiyuan 030001, Shanxi, China
[10]Department of Obstetrics and Gynecology, NYU Langone Health, 550 First Avenue, New York, NY 10012, USA
[11]Institute of Translational Medicine, Tianjin Union Medical Center, Nankai University, Tianjin 300000, China
[12]These authors contributed equally
[13]Lead contact
*Correspondence: bxhjj@163.com (X.B.), shang.wei@163.com (W.S.), wuxueqq@hotmail.com (X.W.), liulin@nankai.edu.cn (L.L.)
https://doi.org/10.1016/j.xcrm.2025.102424

SUMMARY

Fertility in women decreases with age, but the molecular basis for age-related, unexplained infertility remains elusive. Here, we reveal distinct transcriptome changes in oocytes and surrounding cumulus cells from women in their mid-thirties, as evidenced by notably increased transcription of ribosome genes. Additionally, meiosis genes and actin and cohesin components are downregulated in oocytes with age. Lysosomes and proteostasis are also disrupted in cumulus cells. Moreover, DNA hypomethylation and altered heterochromatin deposition at specific genomic loci are linked to increased transcription of ribosome genes. Rapamycin effectively reduces translation and promotes protein homeostasis in cumulus cells. Remarkably, short-term rapamycin allows patients who fail repeated *in vitro* fertilization cycles with embryo developmental arrest to achieve high-quality blastocysts that yield successful pregnancy and live birth. These data suggest a causal role for elevated transcription of ribosome genes in aging oocytes and cumulus cells and identify rapamycin as a promising treatment for age-related infertility. This study is registered at Chinese Clinical Trial Registry (ChiCTR2300069828).

INTRODUCTION

The age-related decline in female fertility is attributable primarily to oocyte quality,[1] which impairs embryo development and causes repeated *in vitro* fertilization (IVF) failures. In human oocytes, chromosome segregation errors increase with age, especially after the mid-thirties. Meiotic defects leading to embryonic aneuploidy are the prime driver of reproductive aging in women.[2–6] Factors contributing to aneuploidy include precocious separation of sister chromatids, chromosome misalignment, spindle disruption, and deficient spindle checkpoints.[3–8] Embryos resulting from the fertilization of aneuploid oocytes typically arrest during development or miscarry.[9] The rate of chromosome segregation errors accelerates from 35 years of age onward.[5]

In addition to chromosome aneuploidy, the DNA damage response, oxidative stress, mitochondrial dysfunction, telomere attrition, autophagy, inflammation, and fibrosis also contribute to ovarian aging.[10–15] The human ovary contains several cell types, particularly oocytes and surrounding cumulus cells.[16,17] Cumulus and granulosa cell connections enable bidirectional communication with oocytes. These proteins involved in bidirectional communication are essential for normal folliculogenesis and germ cell development.[18,19] DNA methylation provides another hallmark of cellular aging (epigenetic aging clocks), enabling estimation of biological age for most tissues across the entire life course.[20,21] Epigenetic aging clocks used to accurately predict biological age have been identified in somatic cells but are more complex in the context of oocyte aging.[22]

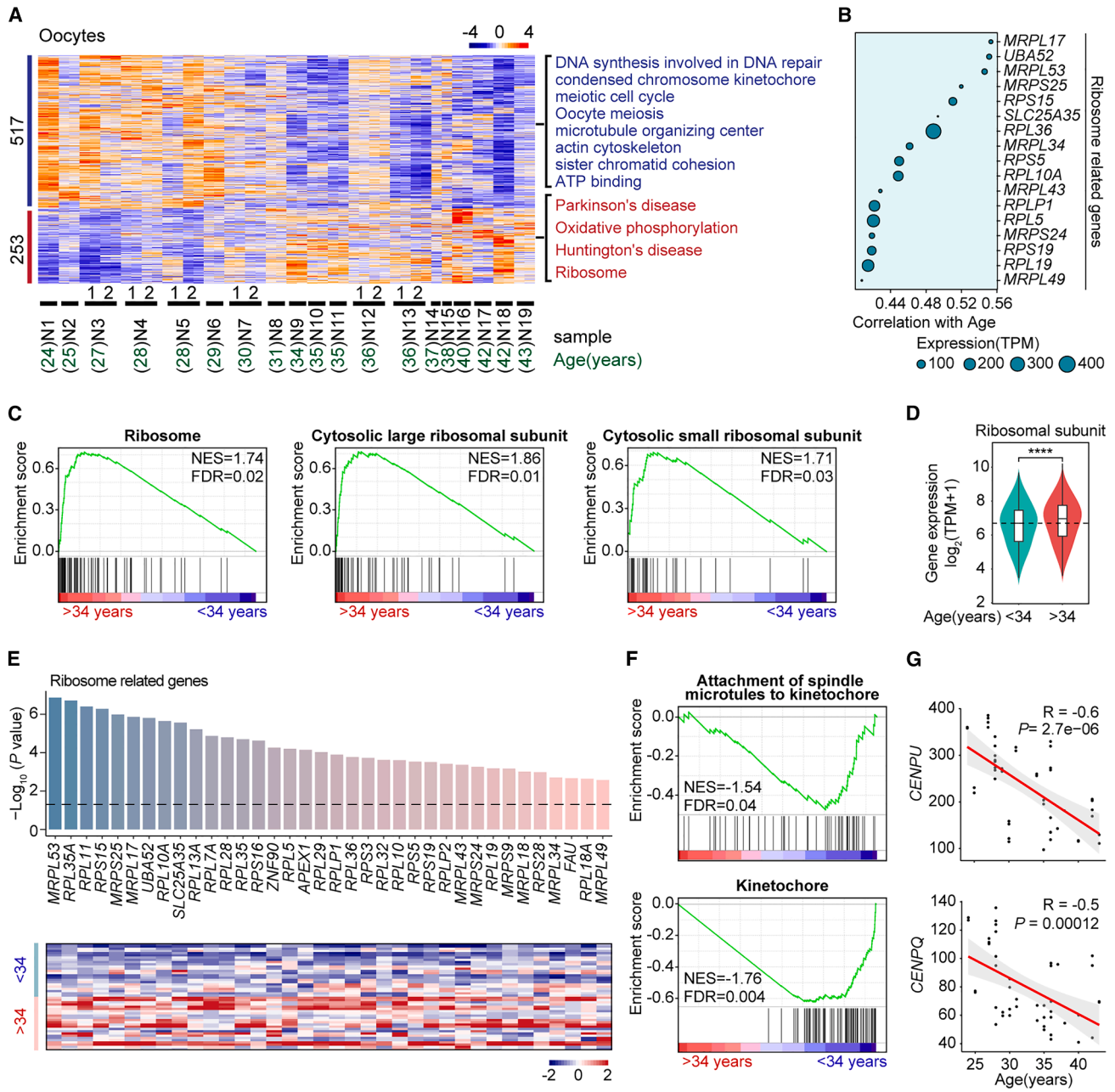

Figure 1. Age-related transcriptome changes in single oocytes

(A) Heatmap showing the expression signatures of specifically expressed genes in oocytes with increasing age, and aging-specific genes were identified based on age-gene expression correlation, with an absolute correlation coefficient cutoff of $|r| \geq 0.4$ and statistical significance (adjusted p value < 0.05). The value for each gene is the row-scaled Z score, and the color key from blue to red indicates the relative gene expression level from low to high, respectively. The index number and age of each sample are marked at the bottom of the heatmap; $n = 48$ for the RNA-seq data. Representative enriched terms of aging-related genes are marked on the right.

(B) Pearson correlations between age and the expression levels of genes related to ribosomes in oocytes. The size of the circles represents the expression levels of genes. The gene expression level was quantified as transcripts per million (TPM).

(C) Gene set enrichment analysis (GSEA) indicating that upregulated genes in oocytes >34 years (including 34) were highly enriched in ribosome-related gene sets. Red, upregulated genes in oocytes >34 years; NES, normalized enrichment score; FDR, false discovery rate.

(D) Violin plot displaying the expression of ribosomal subunit-related genes in oocytes from donors >34 years old compared with those <34 years old; genes were obtained from gene sets including cytosolic large and small ribosomal subunits via GSEA.

(E) Heatmap showing the expression levels of key genes related to ribosomes in oocytes from donors <34 years old and donors >34 (including 34) years old. The bar plot shows −log10 (p value), computed in DESeq2 via the Wald test; the black dotted line represents −log10 (0.05).

(legend continued on next page)

Previous single-cell sequencing studies arbitrarily grouped the age as young or old to explore the impact of aging on female oocytes or ovaries.[23–25] Through integrated multi-omics analysis, including transcriptome analysis via correlation analysis with age, the methylome, and the histone modification, we identified molecular changes in aging oocytes and cumulus cells (CCs). Notably, both oocytes and CCs exhibit striking transcriptional changes by age 34 without artificial grouping by age in our study, providing a potential molecular basis for the declining fecundity in women. Both oocytes and CCs display consistently upregulated ribosome genes, which promote protein translation. Notably, the inhibition of translation by rapamycin, which has been approved for routine clinical use as an immunosuppressant, greatly improves fertility in women who previously failed assisted reproduction.

RESULTS

Aging-specific transcriptome profiling of human oocytes and CCs

We obtained 71 oocyte and 114 CC samples from female donors aged 23–48 years who consented to the experiments and multi-omics analysis. With increasing age, the antral follicle count (AFC), the number of follicles >12 mm, the number of oocytes retrieved, and E2 levels decreased, whereas the levels of FSH (follicle-stimulating hormone) and FSH/LH (luteinizing hormone) increased (Figure S1A), which was consistent with the decreasing ovarian reserve with increasing age.[2,26,27] cDNA libraries were constructed, and RNA was sequenced from single oocyte and CC samples via a previously established method[28] (Figures S1B–1E; Table S1). We identified 19,098 genes expressed in oocytes and 28,761 genes expressed in CCs. The RNA sequencing (RNA-seq) data of the oocyte and CC samples were normalized and subjected to Pearson's correlation analysis. We attempted various age-correlation coefficient cutoffs, based on the principle described[29,30] (also see method details section), and showed that the cutoff of $|r| \geq 0.4$ (for oocytes) or $|r| \geq 0.5$ (for CCs) produced significant differences (adjusted p value < 0.05) between the age and gene expression levels (Tables S2 and S3). Notably, a distinct shift in oocyte gene expression profiles emerged around the age of 34, and this transition involved 517 downregulated and 253 upregulated genes in older compared to younger oocytes (Figure 1A). Analysis of Kyoto Encyclopedia of Genes and Genomes pathways and Gene Ontology (GO) for genes upregulated with age revealed several key pathways, such as Parkinson's disease, Huntington's disease, oxidative phosphorylation, and ribosome-associated genes (e.g., *RPS15*, *RPL36*, and *RPS5*) (Figures 1A and 1B). Additionally, we took advantage of an independent transcriptome dataset of a large cohort of oocytes from women of varying reproductive age[15] and validated the noticeable transition of gene expression profiles around the age of 34 by the age-correlation coefficient cutoff of $|r| \geq 0.4$ (adjusted p value < 0.05) (Figure S1F). Moreover, the independent dataset also revealed the enrichment of ribosome signaling with age and upregulated expression of ribosome-related genes in older oocytes (Figures S1F and S1G), consistent with our findings. The robust replication across the datasets strengthens the association between ribosome dysregulation and oocyte aging.

Gene set enrichment analysis (GSEA) further demonstrated the upregulation of ribosome genes in oocytes from women older than 34 years (Figures 1C–1E). The downregulated genes in older oocytes beyond the age of 34 were enriched for important terms related to meiosis, including centromere kinetochores (*CENPs*), microtubule-organizing centers, the actin cytoskeleton, sister chromatid cohesion, as well as DNA repair (Figures 1A and 1F). Meiotic deficiency with increasing age has been reported previously,[31–33] validating the single-cell RNA-seq analysis reported here. Correlation analysis revealed that key genes, such as *CENPU* and *CENPQ*, were negatively correlated with age (Figure 1G). F-Actin nucleates on chromosomes and coordinates their capture by microtubules in oocyte meiosis.[34] CENPU constitutes the centromere and facilitates the kinetochore-microtubule attachment necessary for the correct separation of chromosomes.[35,36] Prematurely separated chromosomes, associated with loss of cohesion with increasing maternal age, are prone to incorrect segregation during anaphase and contribute to embryo aneuploidy.[4,37]

Aging-specific transcriptional changes in CCs are more pronounced than those in oocytes, including 2,181 genes whose expression is downregulated and 396 genes whose expression is upregulated with maternal age (Figure 2A). The signaling pathways enriched with the downregulated genes included the lysosome (e.g., *CLTA*, *HEXB*, and *GLB1*) (Figure 2B), the proteasome, and metabolic pathways (e.g., purine metabolism, pyrimidine metabolism, and fatty acid metabolism). The upregulated genes were also enriched for the ribosome, in addition to the glycolysis/gluconeogenesis and transforming growth factor β signaling pathways (Figure 2A). Moreover, GSEA revealed that ribosome gene sets were upregulated and lysosome gene sets were downregulated with age (Figures 2C and 2D). Additionally, genes involved in the response to oxidative stress were downregulated with age (Figure 2E). The expression of *GPX4*, an antioxidase that strongly inhibits lipid oxidation, was decreased in aging primate ovaries[14] and noticeably decreased with maternal age in human CCs (Figure 2E).

Integration of translation and ribosome-related GO enrichment and genes by Cytoscape revealed that in both oocytes and CCs, genes related to ribosomes and translation increased in expression with age (Figures 2F and 2G). Gene sets for both the cytosolic large and small ribosomal subunits were significantly enriched for upregulated genes in aging oocytes and

(F) Gene sets related to the attachment of spindle microtubules to kinetochores and to kinetochores themselves were enriched with downregulated genes in oocytes >34 years old.

(G) Correlations between female age and the expression (TPM) of kinetochore-related genes, such as *CENPU* and *CENPQ*, and the correlation coefficient were computed via the Pearson method. Statistical significance is defined as $p < 0.05$.

For (D), violin plot shows the kernel density of the data with box in middle representing the median, the 25% and 75% interquartile range (IQR), and the ±1.5 IQR; p value was calculated by two-tailed unpaired t test; (G) Pearson correlation. ****$p < 0.0001$.

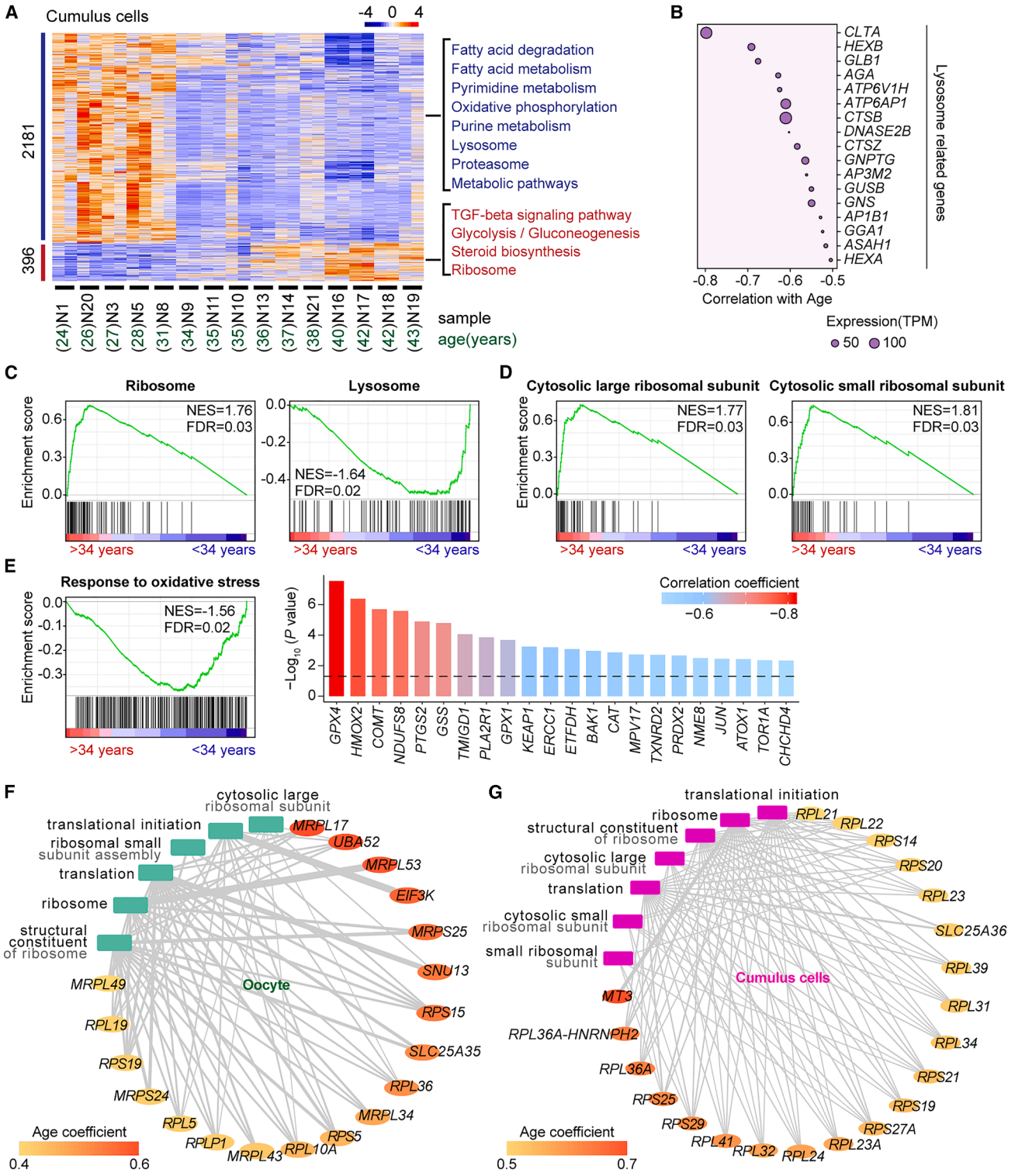

Figure 2. Age-induced changes in the transcriptome of CCs

(A) Heatmap showing the expression signatures of genes specifically expressed in CCs with age, and aging-specific genes were identified based on age-gene expression correlation, with an absolute correlation coefficient cutoff of $|r| \geq 0.5$ and statistical significance (adjusted p value < 0.05). $n = 30$ RNA-seq data points. Representative enriched terms of aging-related genes are marked on the right.

(B) Pearson correlations between age and the expression levels of genes related to lysosomes in CCs.

(legend continued on next page)

CCs (Figures 1C and 2D). Additionally, oocytes expressed genes encoding mitochondrial ribosomal proteins, including *MRPL17*, *MRPL53*, *MRPS25*, *MRPL34*, *MRPL43*, *MRPS24*, and *MRPL49*, which are involved in the composition of mitochondrial ribosomes and protein synthesis within the mitochondrion (Figure 2F).

Together, oocytes and the surrounding CCs display distinct transcriptome changes around the mid-thirties, when age-related fertility loss accelerates.

Ribosome dysregulation and disruption of protein homeostasis in CCs

Increased expression of ribosome genes has not been reported previously in association with oocyte or ovarian aging. Furthermore, when we compared RNA-seq data between relatively older and younger women under the age of 34, the vast majority of genes related to cytosolic large and small ribosomal subunits presented increased expression in both CCs and oocytes from older women (Figures 1D and 3A). Nucleoli are the nuclear structures responsible for ribosome biogenesis, and an enlarged nuclear area and a reduced number of nucleoli are associated with premature aging.[38] We evaluated the nucleolar area as defined by nucleolin staining in CCs. An increase in total nucleolar area (Figures 3B and 3C) and a decrease in nucleolar number were observed in aged CCs (Figure 3D). Additionally, we quantified the levels of 28S and 18S ribosomal RNAs (rRNAs). The content of 18S and 28S rRNAs increased with age in CCs (Figure 3E). Consistently, oocytes from reproductively aged mice displayed increased ribosome numbers associated with altered nucleolar architecture.[39] Taken together, these results suggest that ribosome components and associated translation could increase in CCs with age.

Mechanistic target of rapamycin (mTOR) tightly regulates protein synthesis and autophagy by phosphorylating substrates.[40] The aging of CCs was accompanied by an increase in p-mTOR protein and a decrease in the autophagy-related protein LC3-II (Figure S2A). L-homopropargylglycine incorporation for protein synthesis assays further confirmed that protein synthesis increased significantly in aging CCs (Figure S2B). To further verify ribosome and protein synthesis dysregulation, rapamycin was utilized to inhibit ribosome biogenesis and protein synthesis via mTOR.[41] Additionally, cycloheximide is commonly used to inhibit protein synthesis. Notably, 0.5 μM rapamycin effectively attenuated the increase in protein synthesis induced by aging CCs (Figure S2C). Moreover, senescence-associated β-galactosidase activity was suppressed in aged CCs after rapamycin or cycloheximide treatment (Figure 3F).

Additionally, RNA-seq revealed decreased expression of lysosome- and proteasome-related genes with age (Figures 2A and 3G). We used LysoTracker to label lysosomes and detected that the activity of lysosomes indeed dramatically decreased with age (Figures 3H and S2D). Aberrant expression of ribosomal and lysosome-related genes with age may disrupt protein homeostasis. To examine proteostasis, we performed fluorescence analysis with Proteostat dye in CCs of different ages. Proteostat becomes highly fluorescent upon binding to the amyloid-type β sheet tertiary structure of protein aggregates.[42] Compared with young CCs, aging CCs displayed increased fluorescence of Proteostat (Figures 3I and S2E). The protein aggregates were only slightly increased in oocytes with increasing age (Figure S2F). The accumulation of protein aggregates in aging CCs may imply increased protein synthesis and/or decreased protein degradation, which could be linked to the upregulation of ribosome-related genes and the downregulation of lysosome-related genes, disrupting protein homeostasis.

Age-associated dynamics of the DNA methylome in oocytes and CCs

The epigenetic clock resulting from DNA methylation underlies somatic aging.[20,21,43,44] To understand the molecular mechanisms underlying the changes in the transcriptome with age, we performed low-input post-bisulfite adaptor tagging DNA methylation sequencing to delineate the DNA methylome of oocytes or CCs. A cohort of females was recruited (Table S1) and divided into old (>34 years) and young (<34 years) groups on the basis of transcriptome analysis. Two independent biological replicates per age group were assessed, and robust data were obtained for all the oocyte samples, with reproducible replicates (Figure S3A). A total of 112,510,677 reads per group and approximately 11,259,424 CpGs in the human genome were covered in each sample (Table S4). In general, aging led to a slight increase in DNA methylation in oocytes (Figure S3B), and old oocytes contained a slightly greater proportion of highly methylated sequences than did young oocytes (Figures S3C–S3G).

We observed a peak of differentially methylated regions (DMRs) located immediately upstream and downstream of transcription start sites (Figure S3H). The majority of DMRs were located in transposable element (TE) and intergenic and intronic regions, whereas the promoter and exon regions contained 409 and 373, respectively, of the DMRs, with far more hypermethylated than hypomethylated DMRs (Figure S3I). The methylation levels in older oocytes were greater than those in younger oocytes in terms of genomic features, including 3′ UTRs, exons, intergenic regions, introns, promoters, and TEs (Figure S3J). Moreover, the DMRs of genes were enriched mainly in important signaling pathways, such as the cAMP, oxytocin, and calcium signaling pathways (Figure S3K). Furthermore, association

(C and D) GSEA highlighting that upregulated and downregulated genes in CCs >34 years old were enriched in gene sets related to ribosomes and lysosomes, respectively.

(E) Response to oxidative stress was significantly enriched in downregulated genes in CCs from individuals >34 years old. Key genes are shown in a bar plot, and the color key indicates the correlation coefficient, which was calculated via the Pearson method on the basis of female age and gene expression levels. The vertical axis represents −log10 (*p* value); the black dotted line indicates −log10 (0.05).

(F and G) Integration of translation- and ribosome-related GO enrichment and genes by Cytoscape in female oocytes (F) and CCs (G). Rectangles represent GO enrichment, and ovals represent genes associated with GO enrichment. The color key from yellow to orange indicates the age coefficient from low to high, respectively. The age coefficient was calculated via Pearson correlation between the donor age and gene expression level (TPM) via "cor" in R software. The width of the edge indicates betweenness, reflecting the amount of control that this node exerts over the interactions of other nodes in the network.

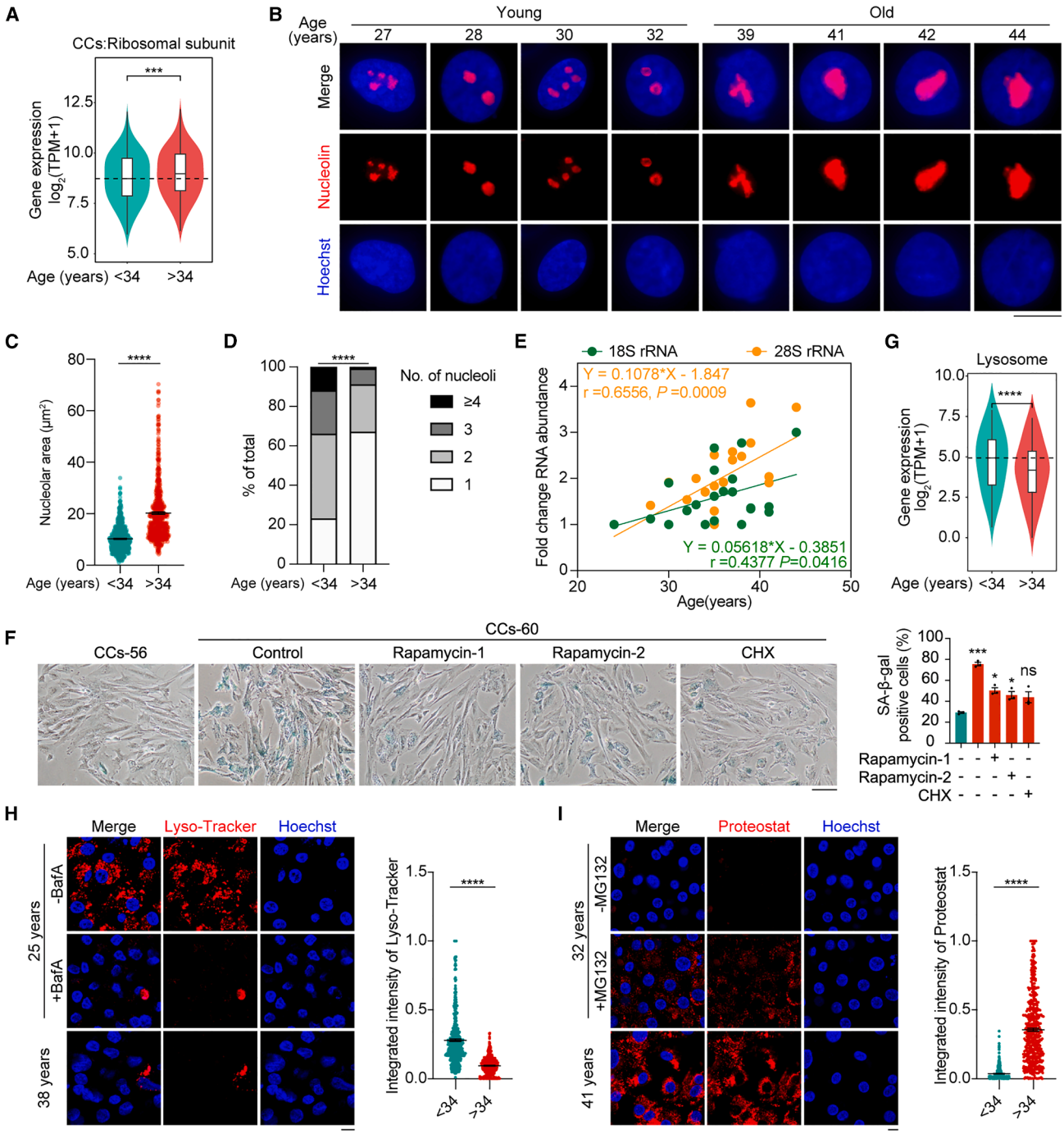

Figure 3. Ribosomes and lysosomes in aging human CCs

(A) Violin plot showing the expression of ribosomal subunit-related genes in CC samples from donors >34 years (including 34) compared with those from donors <34 years old. Genes were obtained from gene sets, including large and small cytosolic ribosomal subunits, via GSEA.

(B) Representative immunofluorescence image of the nucleolar protein nucleolin (red) in CC samples of different ages from four independent experiments. Scale bar, 10 μm.

(C) Comparison of nucleolar area between the <34-year-old and >34-year-old groups. The total area of nucleolar cross-sections per CC was determined by boundaries of nucleolin immunofluorescence. *n* = 600 cells, and each CC sample contained 100 cells. A total of 6 CC samples from 6 women in each age group were collected (5 independent experiments).

(D) Comparison of the percentages of the number of nucleoli between the <34-year-old and >34-year-old groups. The calculated data are shown as percentages (%), *n* = 600 cells. The color depth of the histogram represents the number of nucleoli.

(legend continued on next page)

analysis of the transcriptome and methylation revealed several important genes potentially regulated by methylation, such as *RPS15*, which were hypomethylated and upregulated in old oocytes compared with young oocytes (Figure S3L). Conversely, *CUL4B* was hypermethylated and downregulated in old oocytes compared with young oocytes (Figure S3L). *CUL4B*, a component of the cullin-ring finger ligase-4 complex, is involved in germ cell development and maternal reprogramming, and depletion of *CUL4B* markedly decreases endogenous 5-hydroxymethylcytosine levels.[45]

Overall, there were no or only minimal changes in DNA methylation in CC samples with age (Figures S4A–S4C), which differed from what was observed in oocytes. Moreover, CCs presented greater DNA methylation than did oocytes (Figures S4B and S4C versus Figures S3B and S3C). The DMRs in CC samples between the young and old groups were far less numerous than those in oocytes (Figures S4D versus S3D), contained 2,398 DMRs hypermethylated and 2,227 DMRs hypomethylated in old CC samples (Figure S4E), and were enriched in several signaling pathways, including the mitogen-activated protein kinase and gonadotropin-releasing hormone (GnRH) signaling pathways (Figure S4F). Furthermore, the methylation levels of the promoters and gene bodies of ribosome-related genes decreased with age (Figure S4G).

Many DMRs are located on TEs, and TE expression in both oocytes and CCs changes with increasing age (Figures S5A–S5E), in particular, long interspersed nuclear element 1 (L1) is markedly upregulated in aged CCs in association with decreased DNA methylation of L1 (Figures S5F and S5G). Quantitative reverse-transcription PCR analysis further confirmed that L1 RNA levels in CCs increased with age and that the azidothymidine (AZT, L1 inhibitor) inhibited this increase (Figure S5H). Moreover, the suppression of L1 expression by AZT reduced DNA damage, as evidenced by decreased 53BP1 foci (Figure S5I), supporting the notion that DNA damage represents one of the phenotypes of aging CCs. Notably, many L1 retrotransposons are located very close to ribosome-related genes (*RPS5* and *RPL36A*) (Figure S5J). We also analyzed previously published RNA-seq data from mouse embryonic stem cells[46] and reported that LINE1 RNA knockdown resulted in decreased expression of ribosome-related genes (Figure S5K), which were upregulated in aging CCs. These data suggest a link between L1 and several ribosome-related genes.

In short, the methylation of CCs also changes with age. The elevated expression of some ribosome genes and L1 is associated with decreased DNA methylation.

Ribosome dysregulation and alteration of heterochromatin in CCs

The level of heterochromatin also changes with age.[47] We examined changes in the heterochromatin of CCs, which are typically marked by H3K9me3 and H3K27me3. H3K9me3 immunofluorescence in CCs decreased with increasing maternal age (Figure 4A). Loss of heterochromatin has also been reported in human prophase I-arrested oocytes with age.[48] However, H3K27me3 immunofluorescence intensity did not differ between young and old CCs (Figure S6).

To reveal genome-wide enrichment of H3K9me3, we performed CUT&Tag of H3K9me3 in CCs from young and older women. The overall abundance of H3K9me3 in the genome decreased with age (Figure 4B). H3K9me3 enrichment at promoters also decreased with maternal age (Figure S7A). H3K9me3 was primarily enriched in intergenic regions, with its enrichment at distal intergenic region slightly decreasing with age (Figure S7B). Moreover, H3K9me3 peaks were found with a specific distribution with age, including 9,999 young-specific H3K9me3 peaks that decreased with age and 17,208 old-specific H3K9me3 peaks that increased with age (Figure 4C). Through correlation analysis, these peaks were highly correlated within the group but differed between young and older CCs (Figure S7C).

The young-specific H3K9me3 peaks were detected in genes related to misfolded protein binding, preribosome, regulation of ribonucleoproteins, and rRNA processing, which are involved in ribosome biogenesis, and the H3K9me3 enrichment on these genes was lower in old CCs than in young CCs (Figures 4D and 4E). In contrast, genes marked by old-specific H3K9me3 peaks were associated with protein localization to microtubules, negative regulation of cytoplasmic translation, regulation of cell proliferation, and oxidoreductase activity (Figure 4D). The old-specific H3K9me3 peaks enriched in genes related to the negative regulation of cytoplasmic translation were reduced in young CCs

(E) Abundance of 18S and 28S rRNAs determined by qPCR in CC samples from donors of varying ages (n = 22; 24–44 years), normalized to GAPDH mRNA. The coefficient was calculated via Pearson's correlation, and the p values for 18S and 28S rRNA abundance changes with age are shown.
(F) SA-β-gal staining of female CCs (CCs-56, 26 years and CCs-60, 37 years) treated with or without rapamycin (−1: 0.25 μM and −2: 0.50 μM) or CHX (cycloheximide, 0.30 μM) for 3 days. Scale bar, 100 μm. n = 3 (for each independent experiment, 20 visual fields were randomly selected for statistical analysis).
(G) Violin plot showing the expression of lysosome-related genes (17 genes) in CC samples from donors >34 years compared with those <34 years. Lysosome-related genes were selected from lysosomes via Kyoto Encyclopedia of Genes and Genomes (KEGG) analysis and met the criterion of an age coefficient of at least −0.5.
(H) Representative immunofluorescence images of CC samples from donors of varying ages stained with LysoTracker (red, acidic organelles; lysosomes) and Hoechst (blue, nuclei). The cells were treated with the lysosome inhibitor bafilomycin A (BafA, 700 nM) for 6 h as a control. Scale bar, 10 μm. Right: the integrated intensity of LysoTracker fluorescence was estimated by ImageJ; n = 480; each sample contained 80 cells, with a total of 6 independent samples per group (5 independent experiments).
(I) Representative immunofluorescence images of CC samples from donors of varying ages stained with Proteostat (red, protein aggregates) and Hoechst (blue, nuclei). The cells were treated with the proteasome inhibitor MG132 (10 μM) for 12 h as a control. Scale bar, 10 μm. Right: integrated intensity of Proteostat fluorescence estimated with ImageJ; n = 480; each sample contained 80 cells, with a total of 6 independent samples per group (5 independent experiments).
(C, F, H, and I) Data are represented as mean ± SEM. (C, H, and I) Mann-Whitney test; (F) ANOVA tests for multiple comparisons; (A and G) violin plot shows the kernel density of the data with box in middle representing the median, the 25% and 75% interquartile range (IQR), and the ±1.5 IQR; p value was calculated by two-tailed unpaired t test; (D) chi-squared test; (E) Pearson correlation. *p < 0.05, ***p < 0.001, and ****p < 0.0001.

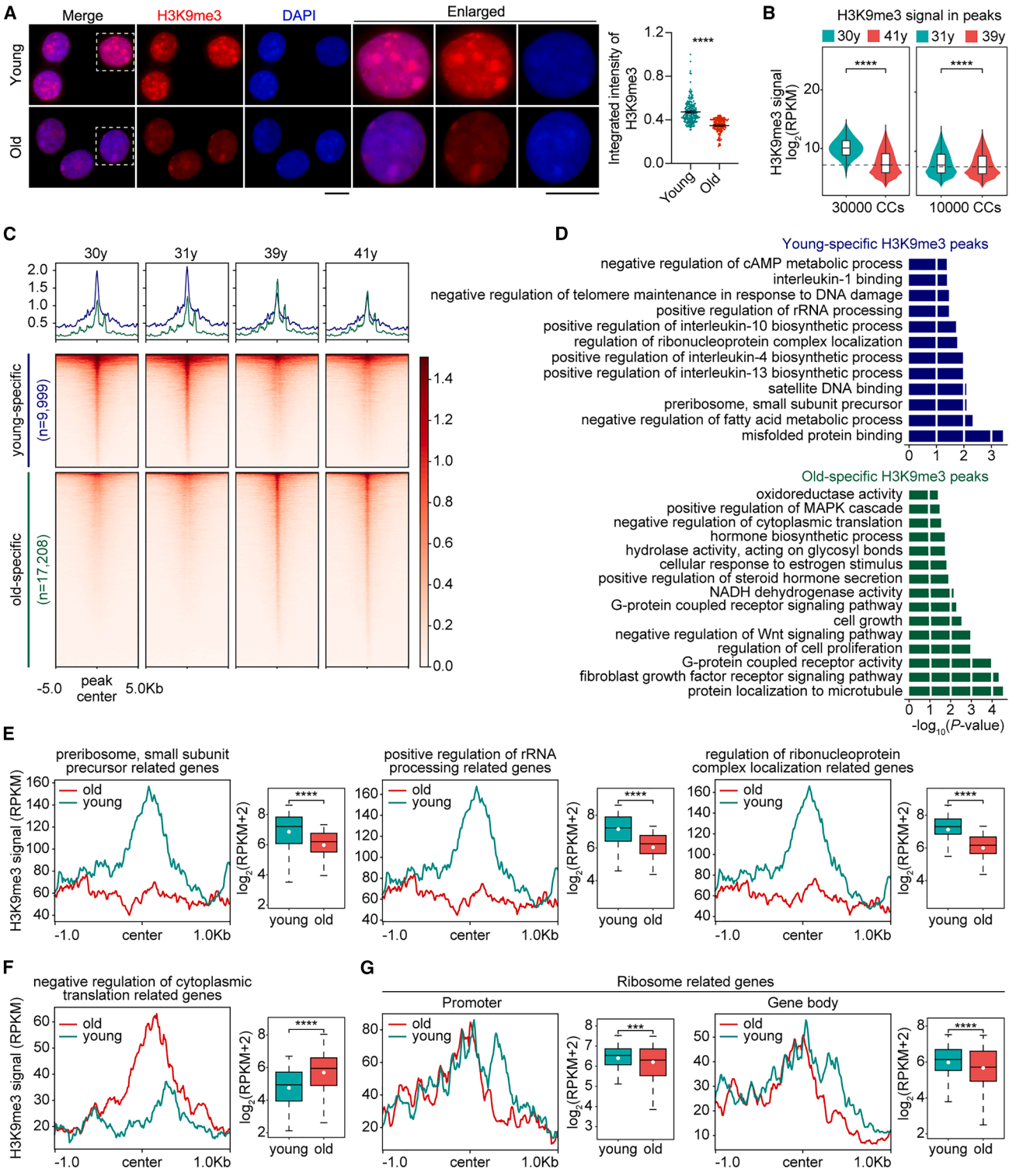

Figure 4. H3K9me3 abundance on ribosome genes decreases with age

(A) Immunostaining of H3K9me3 (red) in CCs (Passage 2) from young women and women of advanced reproductive age. Scale bars, 10 μm. *n* = 200 cells (from three young donors aged 28, 31, and 31 years or three older donors aged 38, 39, and 43 years).

(B) Violin plots displaying the normalized signal of H3K9me3 at peaks identified by CUT&Tag in CCs collected from two repeated experiments, including paired young and relatively old women (30 vs. 41 or 31 vs. 39 years old).

(C) H3K9me3 enrichment around young-specific and old-specific H3K9me3 peaks.

(legend continued on next page)

(Figure 4F). Furthermore, H3K9me3 enrichment at the promoter and gene body of ribosome-related genes was reduced in the old CCs (Figure 4G). The altered H3K9me3 enrichment in these terms implied that the transcriptional inhibition of H3K9me3 on ribosomal biogenesis- and translation-related genes may be abrogated during aging, corroborating the increased transcription of ribosomal genes and potential promotion of translation.

Werner syndrome is a premature aging disorder caused by WRN protein deficiency. We analyzed the H3K9me3 chromatin immunoprecipitation sequencing data of *WRN*$^{-/-}$ hMSCs (human mesenchymal stem cells) published previously.[49] Consistently, H3K9me3 enrichment on ribosome-related genes was reduced in *WRN*$^{-/-}$ hMSCs (Figure S7D), accompanied by increased expression of ribosome-related genes (Figure S7E). Furthermore, CCs treated with chaetocin (H3K9me3 inhibitor)[50] exhibited upregulated expression levels of ribosome-related genes, such as *RPS19*, *RPL22*, and *RPL36A* (Figure S7F). Combined with the aforementioned results, the changes in the expression of ribosome-related genes during aging can be regulated by alterations in heterochromatic H3K9me3.

The lysosome-related genes presented increased H3K9me3 enrichment in gene body regions, whereas promoter regions did not change with age (Figure S7G), which was correlated with downregulation of lysosome-related genes. In addition, genes related to oxidoreductase activity were enriched with the old-specific H3K9me3 peak (Figures 4D and S7H) and were downregulated with age (Figures S7I and S7J). These data suggest that H3K9me3 enrichment at specific loci with increasing age may influence the expression of genes related to lysosomes and oxidoreductase activity in CCs.

Rapamycin intervention in reproductively aged mice

Upregulation of ribosome-related entries was identified in old mouse oocytes by comparative transcriptome analysis with young oocytes, suggesting that ribosome dysregulation was conserved between human and mouse oocytes during aging (Figures S8A and S8B). We identified 53 ribosome-related genes upregulated in aged mouse oocytes (Figure S8C) and five ribosome-related genes, similar to those in human oocytes, including *Rps5*, *Mrps24*, *Mrpl53*, *Rpl36*, and *Rpl5* (Figure S8D).

We took advantage of rapamycin to inhibit mTOR and translation to explore its potential function in delaying aging. Oocytes and CCs were collected from the ovaries of young (2-month-old) and old (10-month-old) mice (Figure S9A). Rapamycin at 0.5 μM blocked the increased phosphorylation of 4E-BP1 and S6 in old CCs, which regulated translation and ribosome biogenesis (Figures S9B and S9C). Furthermore, rapamycin inhibited the activity of SA-β-gal and the increase in reactive oxygen species (ROS) levels in old CCs (Figures S9D and S9E). The elevated p-S6 protein level in aged oocytes during *in vitro maturation* (IVM) was also decreased by rapamycin (Figure S9F), whereas the S6 protein level did not change (Figure S9G). Moreover, rapamycin promoted the rate of IVM (Figure S9H) and reduced ROS levels in aging oocytes (Figure S9I). Additionally, the rates of disrupted spindles and chromosome misalignment were elevated in aging oocytes, and rapamycin alleviated these abnormalities (Figure S9J). Hence, rapamycin treatment effectively delays the aging of oocytes and CCs.

Rapamycin improves embryo development and pregnancy

We tested whether rapamycin can improve oocyte quality, subsequent embryo development, and clinical pregnancy. A randomized controlled clinical trial was conducted. A total of 122 women underwent screening, and 100 met the eligibility criteria. The 100 women who provided informed consent were randomly assigned to the control group or rapamycin group, with 50 patients in each group (Figure 5A). After randomization, patients in the control group received a standardized GnRH agonist long protocol, whereas patients in the rapamycin group received a standardized GnRH agonist long protocol plus rapamycin treatment for 21–28 days from the day of endogenous hormone downregulation until the oocyte retrieval day. Previous clinical trials of rapamycin and aging used doses of approximately 0.5–2.0 mg for 8 or 12 weeks.[51,52] In our trial, patients in the rapamycin group received 1 mg rapamycin orally daily for 21–28 days. Three patients in the control group and five patients in the rapamycin group did not have oocytes after controlled ovarian hyperstimulation according to the protocol.

Among the remaining patients, 19 patients underwent IVF, and 28 patients underwent intracytoplasmic sperm injection (ICSI) in the control group. In the rapamycin group, 12 patients underwent IVF, and 33 patients underwent ICSI. There were no significant differences in baseline variables between patients undergoing IVF or ICSI in either the control or rapamycin groups (Figures S10A and S10B), especially in indicators related to embryologic characteristics such as the number of zygotes and embryos. Therefore, the effect, if any, of different fertilization procedures was minimal for our subsequent analysis.

Notably, significantly more zygotes, embryos, and good-quality embryos were obtained in the rapamycin group than in the control group (median value, zygotes: 3.0 vs. 2.0, $p = 0.012$; embryos: 2.0 vs. 1.0, $p = 0.001$; and good-quality embryos: 2.0 vs. 1.0, $p < 0.001$) (Figures 5B and 5C). The number of metaphase II oocytes retrieved and baseline variables, including anti-mullerian hormone (AMH), FSH, and AFC, did not differ

(D) Functional enrichment analysis of genes marked by young-specific (upper) and old-specific (lower) H3K9me3 peaks.
(E) Normalized signals of H3K9me3 peaks identified from genes associated with ribosome biogenesis included preribosomes, small subunit precursors, positive regulation of rRNA processing, and regulation of ribonucleoprotein complex localization in young (30 and 31 years) and old (39 and 41 years) CCs. The center indicates the center of the peaks. Right, the boxplot showing the signal of H3K9me3 enrichment.
(F) Normalized signals of H3K9me3 peaks identified from genes related to the negative regulation of cytoplasmic translation in young and old CCs.
(G) Normalized signal of H3K9me3 peaks in young and old CCs identified from promoters (±1,000 bp around the TSS) and gene bodies (from the TSSs to the TESs) associated with upregulated ribosome-related genes identified via RNA-seq.
(A) Data are represented as mean ± SEM. (B) Violin plot shows the kernel density of the data with box in middle representing the median, the 25% and 75% interquartile range (IQR), and the ±1.5 IQR. (E–G) Box represents the median, the 25% and 75% IQR, and the ±1.5 IQR. (A, B, and E–G) Two-tailed unpaired *t* test. ***$p < 0.001$ and ****$p < 0.0001$.

A

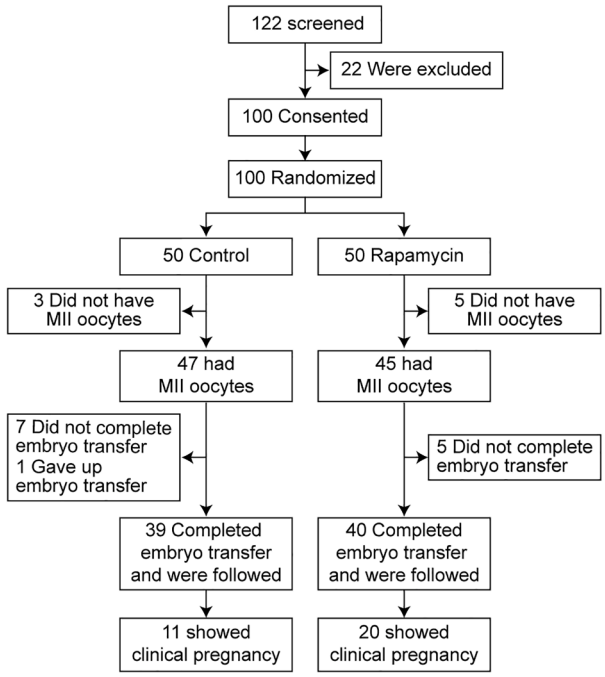

B

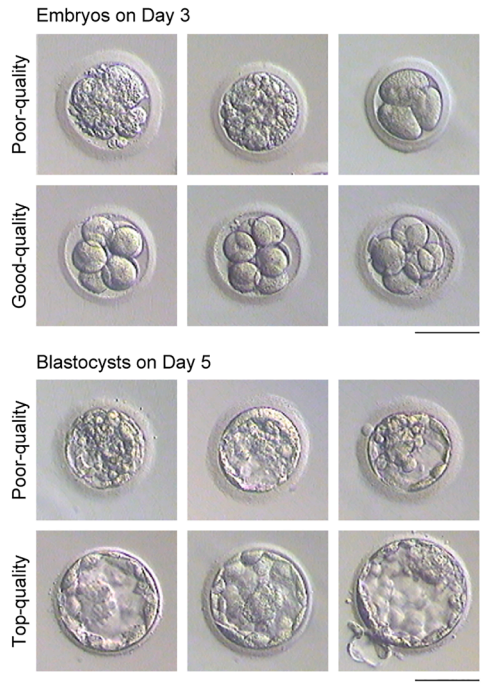

C

Table 1. Outcomes of controlled ovarian hyperstimulation

Characteristic	Rapamycin (N = 50)		Control (N = 50)		*P* value
	No. of Patients	Value	No. of Patients	Value	
Age — yr	50	36.4 ± 4.9	50	34.8 ± 4.7	0.095
AMH (ng/mL)	50	0.98 ± 0.87	50	0.97 ± 0.72	0.743
FSH (mIU/mL)	50	12.57 ± 5.49	50	12.55 ± 4.99	0.850
AFC (n)*	50	5 (4, 7)	50	5 (4, 6)	0.443
No. of MII oocytes retrieved*	45	3 (1, 4)	47	2 (1, 3)	0.108
No. of zygotes*	45	3 (2, 4)	47	2 (1, 3)	0.012
No. of embryos on day 3*	45	2 (1, 3)	47	1 (1, 2)	0.001
No. of good-quality embryos on day 3*	45	2 (1, 3)	47	1 (0, 1)	< 0.001
No. of blastocysts on day 5-6*	21	2 (2, 2)	12	1 (1, 1)	0.012
No. of top-quality blastocysts on day 5-6*	21	1 (0, 2)	12	0 (0, 0)	0.043

D

Table 2. Outcomes of clinical pregnancy

Outcome	Rapamycin (N = 50)	Control (N = 50)	Absolute Difference between Groups (95% CI)	Risk Ratio in Rapamycin Group (95% CI)	*P* value
No. of patients undergone ET	40	39	—	—	—
Day 3	20	28	—	—	—
Day 5-6	20	11	—	—	—
No. of clinical pregnancy (%)	20/40 (50.0)	11/39 (28.2)	21.8 (0.8 to 42.8)	1.77 (0.98 to 3.19)	0.047
Day 3	9/40 (22.5)	8/39 (20.5)	2.0 (−16.1 to 20.1)	1.10 (0.47 to 2.55)	0.830
Day 5-6	11/40 (27.5)	3/39 (7.7)	19.8 (3.6 to 36.0)	3.58 (1.08 to 11.85)	0.021

Figure 5. Rapamycin improves fertility in human IVF clinics

(A) Enrollment and outcomes.

(B) Poor-quality (arrested or fragmented) and good-quality embryos on day 3 (upper); poor-quality and top-quality blastocysts on day 5 (lower); scale bars, 100 μm.

(C) Outcomes of controlled ovarian hyperstimulation in the control and rapamycin groups. The plus-minus values are the means ± SDs. The asterisks indicate the medians (Q1, Q3). Differences between the two groups were calculated via the Wilcoxon test. Embryos were scored according to morphological criteria, with

(legend continued on next page)

between the control and rapamycin groups (Figure 5C). The number and top quality of blastocysts in the rapamycin group were significantly greater than those in the control group (median value, blastocysts: 2.0 vs. 1.0, $p = 0.012$; top-quality blastocysts[55]: 1.0 vs. 0, $p = 0.043$) (Figures 5B and 5C). These results indicate that the addition of rapamycin to patients can effectively improve oocyte quality and subsequent embryo development following the fertilization of retrieved oocytes.

To date, 40 of 45 patients (88.9%) in the rapamycin group and 39 of 47 patients (83.0%) in the control group completed embryo transfer (Figure 5A), and 20 of 40 patients in the rapamycin group and 28 of 39 patients in the control group opted to undergo transfer of day 3 embryos, whereas 20 of 40 patients in the rapamycin group and 11 of 39 patients in the control group opted to undergo transfer of day 5–6 blastocysts (Figure 5D). The decision for embryo transfer largely depended on embryo quality on day 3, when more good-quality 4- to 8-cell embryos were available, and the embryos were subjected to further culture to the blastocyst stage. After embryo transfer, the rate of clinical pregnancy in the rapamycin group was significantly greater than that in the control group (50.0% vs. 28.2%), with a rate ratio of 1.77 (95% confidence interval [CI], 0.98 to 3.19; $p = 0.047$) (Figure 5D). The pregnancy rate might differ between blastocyst-stage (day 5–6) embryo transfer and cleavage-stage (day 3) embryo transfer. Hence, we separately compared the pregnancy rates for patients who underwent day 3 embryo transfer and those who underwent day 5–6 embryo transfer. The clinical pregnancy rate of the patients who underwent day 5–6 blastocyst transfer in the rapamycin group was significantly greater ($p = 0.021$) than that of the control group (27.5% vs. 7.7%; rate ratio, 3.58; 95% CI, 1.08 to 11.85) (Figure 5D). These findings suggest that blastocyst transfer in patients treated with rapamycin can be superior to day 3 embryo transfer in terms of clinical pregnancy. The transfer of top-quality blastocysts to patients receiving rapamycin improved the clinical pregnancy rate.

Furthermore, we tracked the live birth rate, and thus far, 10 of the 14 patients (71.4%) in the rapamycin group who were followed up to their due date had delivered live-born infants, and 6 of the 8 patients (75.0%) in the control group had delivered live-born infants (Tables S5 and S6). Some patients had not yet reached the appropriate date (rapamycin, 6 patients; control, 3 patients), and the current live birth rate did not differ between the rapamycin and control groups. These results, nevertheless, indicate that rapamycin does not negatively impact the live birth rate. The results of clinical trials thus far indicate that rapamycin noticeably increases oocyte and embryo quality and the clinical pregnancy rate. Moreover, the pregnant patients had successful live birth delivery rates at least comparable to those of the controls who did not receive rapamycin, further confirming the safety of rapamycin.

We also examined the protein levels of S6 and p-S6 in CCs collected from patients who received rapamycin compared with those collected from controls who were not treated with rapamycin. Rapamycin indeed reduced p-S6/S6 levels (Figure S10C). Further refinement of the rapamycin dosage and time and duration of treatment may further increase the efficacy of pregnancy and fertility.

DISCUSSION

We propose that elevated transcription of ribosome genes and components and aberrant proteostasis impair oocytes and their surrounding CCs, providing a mechanism to explain age-related poor embryo development and infertility. Transcriptome analysis of single oocytes and CCs from aged women undergoing IVF revealed aberrant upregulation of ribosome genes by the mid-thirties, and this consistent characteristic could be explained by the close interactions and communication between oocytes and CCs. The potential alterations in the state of these two cell types are likely to affect each other, thereby affecting folliculogenesis and oogenesis.[57,58] Mechanistically, the elevated transcription of ribosome genes could be attributable to the loss or reduction of heterochromatin and altered methylation. Indeed, inhibition of H3K9me3 notably increases the expression levels of ribosome-related genes, such as *RPS19*, *RPL22*, and *RPL36A*. *RPL22* is a driver of cellular senescence, promotes the degradation of the heterochromatin proteins HP1γ and KAP1, and stimulates the transcription of rRNA.[59] Interestingly, TORC1 promotes the transcription of rRNA and ribosome-related genes by preventing heterochromatin formation.[60] Aged hematopoietic stem cells and fibroblasts from patients with Hutchinson-Gilford progeria syndrome (premature aging disorders) also exhibit increased expression of ribosomal genes or proteins and rRNA hypomethylation.[38,61] Thus, these previous studies and our findings support the notion that ribosome dysregulation is tightly linked to heterochromatin and DNA methylation during aging.

Our data also confirmed previous findings in oocytes that meiosis, the microtubule and actin cytoskeleton, and cohesion gene expression decrease with maternal age.[4] Defective spindle and actin assembly and chromosome misalignment are linked to high aneuploidy levels in older eggs, contributing to age-related infertility.[62–65] Additionally, the expression of lysosomal genes in CCs decreases with increasing maternal age, and aberrant protein aggregates accumulate. Like in mouse oocytes,[66] human oocytes do not show a significant increase in protein aggregation with age. Protein degradation mechanisms in oocytes might differ from those in CCs, and this warrants further investigation. Our findings that increased transcription of ribosome-related

"good" defined as grade I: a cell number of 7–9, even cell size, less than 10% fragmentation, and no multinucleation. Day-5/6 blastocyst cultures were performed in cases of poor embryo quality or at the request of a patient.[53,54] A top-quality blastocyst-stage embryo is at least in the expanded blastocyst stage (BL3) and has a type A inner cell mass (in which cells are tightly packed, with many cells present) and a trophoectoderm that is either type A (with many cells forming a cohesive epithelium) or type B (with few cells forming a loose epithelium).[55,56]

(D) Outcomes of pregnant patients with or without rapamycin treatment (control). *p* values were calculated via the chi-square test. Clinical pregnancy was defined as the observation of a gestational sac via ultrasonography.

(C and D) Continuous data are represented as the mean ± SD or medians (Q1, Q3); categorical data are represented as frequencies and percentages. (C) Wilcoxon test; (D) chi-square test.

genes is accompanied by increased protein aggregation and disrupted proteostasis in aging CCs are consistent with findings that increased ribosome pausing and collision result in accumulated protein aggregation and impaired proteostasis during aging in *C. elegans* and yeast models.[67] Aging-induced ribosome-related quality control overload may require increased expression of ribosome-related genes, further impairing proteostasis. Ribosomes are maintained in a dormant state and translationally repressed in vertebrate eggs (zebrafish and *Xenopus laevis*) and transition to an active state after fertilization.[68] Notably, ribosome activity is downregulated in the human population with exceptional longevity from Hainan Province, China.[69] Similarly, we show that inhibiting ribosome biogenesis and protein synthesis could abrogate oocyte and CC senescence, improving embryo quality and development and thus pregnancy.

Taken together, increased transcription of ribosome genes is implicated as a potential player in the deterioration of oocyte quality and unexplained infertility with age and can serve as a potential target to improve fertility. Rapamycin, which is commonly employed as an immunosuppressant for organ transplantation and as an anti-aging strategy, may play a role in the treatment of infertility in older women. Some clinical trials on rapamycin and aging have confirmed that oral rapamycin can affect erythrocyte parameters and senescence-associated secretory phenotype-related factors in elderly individuals,[51,52] which reflects the systemic effect of rapamycin on patients. However, in our clinical trial, whether rapamycin improves clinical pregnancy in infertile women is direct or based on systemic effects, and larger and more comprehensive clinical trials are warranted.

Limitations of the study

The clinical implications and translational potential of our findings necessitate further validation in larger patient cohorts. Another limitation is the sample size of the sequencing; however, through multiple sequencing methods, systematic experimental validation, and critical intervention experiments, we have demonstrated that ribosome represents a promising therapeutic target for female infertility.

RESOURCE AVAILABILITY

Lead contact

Further information and requests for resources and reagents should be directed to and will be fulfilled by the lead contact, Lin Liu (liulin@nankai.edu.cn).

Materials availability

This study did not generate new, unique reagents.

Data and code availability

- All the data are available in the main text or the supplemental information. The raw RNA-seq, MethylC-Seq, and CUT&Tag sequencing data generated in this study have been deposited in the Genome Sequence Archive (GSA) of the National Genomics Data Center, China National Center for Bioinformation/Beijing Institute of Genomics, Chinese Academy of Sciences, under accession number HRA005257 (BioProject accession: PRJCA018848), which can be accessed at https://ngdc.cncb.ac.cn/gsa-human/. These data are available under restricted access, as individual genomic sequencing data are protected owing to patient privacy and Regulations on the Management of Human Genetics Resources of China. The raw data can be requested via the GSA-Human System and can be authorized for downloading by the Data Access Committee for research and noncommercial use only. The RNA-seq data for the oocytes and CCs of donors (N8, N13, and N12) were obtained from our previous publication, GSE155489 (GSM4705187–GSM4705192; GSM4705199–GSM4705202). Mouse oocyte RNA-seq data were downloaded from our previous publication (GSE184637).
- This paper does not report original code.
- Any additional information required to reanalyze the data reported in this paper is available from the lead contact upon request.

ACKNOWLEDGMENTS

This work was supported by the China National Key R&D Program (2022YFA1103800), the National Natural Science Foundation of China (91749129, 32030033, 82230052, and 31970667), and the Innovation Plan of Medical Science and Technology of "Four in a batch" (2020TD19). We thank Mo Gou for assisting with the MethylC-Seq library construction experiments, Jiao Yang for helping with some of the experiments, and Zhengmao Zhu for helping with statistics analysis.

AUTHOR CONTRIBUTIONS

J.L. designed the experiments, conducted the major experiments, analyzed the data, and prepared the manuscript. C.L. conducted important mouse experiments and revised the manuscript. H.C. and H.Z. collected the clinical materials and revised the manuscript. Linlin Liu, X.Y., G.F., and Y.W. conducted part of the experiments and discussed the experiments and data analysis. Q.L. provided clinical materials. T.Y. provided the clinical material. X.B. and W.S. provided clinical materials and relevant guidance for clinical diagnosis, discussed the experiments, and revised the manuscript. H.W., P.Z., and X.W. conducted the clinical translational experiments on rapamycin and revised the manuscript. D.L.K. advised the project and revised the manuscript. Lin Liu conceived the project, designed the experiments, and revised the manuscript.

DECLARATION OF INTERESTS

The authors declare no competing interests.

STAR★METHODS

Detailed methods are provided in the online version of this paper and include the following:

- KEY RESOURCES TABLE
- EXPERIMENTAL MODEL AND STUDY PARTICIPANT DETAILS
  - Mice and housing conditions
  - Mouse cumulus cells and culture
  - Ethics statement
  - Human subjects
  - Clinical study design and oversight
  - Clinical study: Inclusion and exclusion criteria
  - Clinical study: Sample size estimation
  - IVF-ET procedures
  - Clinical interventions
  - Clinical outcomes
  - Ovarian stimulation
  - Oocyte retrieval and isolation of cumulus cells
  - Human cumulus cells and culture
- METHOD DETAILS
  - *In vitro* maturation of mouse oocytes
  - ROS assay
  - Immunofluorescence microscopy of mouse samples
  - Immunofluorescence microscopy of human samples
  - Protein synthesis assay
  - AZT treatment
  - Rapamycin and chaetocin treatment

SUPPLEMENTAL INFORMATION

Supplemental information can be found online at https://doi.org/10.1016/j.xcrm.2025.102424.

Received: August 30, 2024
Revised: July 31, 2025
Accepted: October 1, 2025
Published: October 27, 2025

REFERENCES

1. Navot, D., Bergh, P.A., Williams, M.A., Garrisi, G.J., Guzman, I., Sandler, B., and Grunfeld, L. (1991). Poor oocyte quality rather than implantation failure as a cause of age-related decline in female fertility. Lancet *337*, 1375–1377. https://doi.org/10.1016/0140-6736(91)93060-m.
2. te Velde, E.R., and Pearson, P.L. (2002). The variability of female reproductive ageing. Hum. Reprod. Update *8*, 141–154. https://doi.org/10.1093/humupd/8.2.141.
3. Broekmans, F.J., Soules, M.R., and Fauser, B.C. (2009). Ovarian aging: mechanisms and clinical consequences. Endocr. Rev. *30*, 465–493. https://doi.org/10.1210/er.2009-0006.
4. Charalambous, C., Webster, A., and Schuh, M. (2023). Aneuploidy in mammalian oocytes and the impact of maternal ageing. Nat. Rev. Mol. Cell Biol. *24*, 27–44. https://doi.org/10.1038/s41580-022-00517-3.
5. Gruhn, J.R., Zielinska, A.P., Shukla, V., Blanshard, R., Capalbo, A., Cimadomo, D., Nikiforov, D., Chan, A.C.H., Newnham, L.J., Vogel, I., et al. (2019). Chromosome errors in human eggs shape natural fertility over reproductive life span. Science *365*, 1466–1469. https://doi.org/10.1126/science.aav7321.
6. Capalbo, A., Hoffmann, E.R., Cimadomo, D., Ubaldi, F.M., and Rienzi, L. (2017). Human female meiosis revised: new insights into the mechanisms of chromosome segregation and aneuploidies from advanced genomics and time-lapse imaging. Hum. Reprod. Update *23*, 706–722. https://doi.org/10.1093/humupd/dmx026.
7. Webster, A., and Schuh, M. (2017). Mechanisms of Aneuploidy in Human Eggs. Trends Cell Biol. *27*, 55–68. https://doi.org/10.1016/j.tcb.2016.09.002.
8. Hassold, T., and Hunt, P. (2009). Maternal age and chromosomally abnormal pregnancies: what we know and what we wish we knew. Curr. Opin. Pediatr. *21*, 703–708. https://doi.org/10.1097/MOP.0b013e328332c6ab.
9. Qi, S.T., Liang, L.F., Xian, Y.X., Liu, J.Q., and Wang, W. (2014). Arrested human embryos are more likely to have abnormal chromosomes than developing embryos from women of advanced maternal age. J. Ovarian Res. *7*, 65. https://doi.org/10.1186/1757-2215-7-65.
10. May-Panloup, P., Boucret, L., Chao de la Barca, J.M., Desquiret-Dumas, V., Ferré-L'Hotellier, V., Morinière, C., Descamps, P., Procaccio, V., and Reynier, P. (2016). Ovarian ageing: the role of mitochondria in oocytes and follicles. Hum. Reprod. Update *22*, 725–743. https://doi.org/10.1093/humupd/dmw028.
11. Polonio, A.M., Chico-Sordo, L., Córdova-Oriz, I., Medrano, M., García-Velasco, J.A., and Varela, E. (2020). Impact of Ovarian Aging in Reproduction: From Telomeres and Mice Models to Ovarian Rejuvenation. Yale J. Biol. Med. *93*, 561–569.
12. Kasapoglu, I., and Seli, E. (2020). Mitochondrial Dysfunction and Ovarian Aging. Endocrinology *161*, bqaa001. https://doi.org/10.1210/endocr/bqaa001.
13. Ruth, K.S., Day, F.R., Hussain, J., Martínez-Marchal, A., Aiken, C.E., Azad, A., Thompson, D.J., Knoblochova, L., Abe, H., Tarry-Adkins, J.L., et al. (2021). Genetic insights into biological mechanisms governing human ovarian ageing. Nature *596*, 393–397. https://doi.org/10.1038/s41586-021-03779-7.
14. Wang, S., Zheng, Y., Li, J., Yu, Y., Zhang, W., Song, M., Liu, Z., Min, Z., Hu, H., Jing, Y., et al. (2020). Single-Cell Transcriptomic Atlas of Primate Ovarian Aging. Cell *180*, 585–600.e19. https://doi.org/10.1016/j.cell.2020.01.009.
15. Llonch, S., Barragán, M., Nieto, P., Mallol, A., Elosua-Bayes, M., Lorden, P., Ruiz, S., Zambelli, F., Heyn, H., Vassena, R., and Payer, B. (2021). Single human oocyte transcriptome analysis reveals distinct maturation stage-dependent pathways impacted by age. Aging Cell *20*, e13360. https://doi.org/10.1111/acel.13360.
16. Wagner, M., Yoshihara, M., Douagi, I., Damdimopoulos, A., Panula, S., Petropoulos, S., Lu, H., Pettersson, K., Palm, K., Katayama, S., et al. (2020). Single-cell analysis of human ovarian cortex identifies distinct cell populations but no oogonial stem cells. Nat. Commun. *11*, 1147. https://doi.org/10.1038/s41467-020-14936-3.
17. Li, L., Yang, R., Yin, C., and Kee, K. (2020). Studying human reproductive biology through single-cell analysis and in vitro differentiation of stem cells into germ cell-like cells. Hum. Reprod. Update *26*, 670–688. https://doi.org/10.1093/humupd/dmaa021.
18. Chen, J., Torcia, S., Xie, F., Lin, C.J., Cakmak, H., Franciosi, F., Horner, K., Onodera, C., Song, J.S., Cedars, M.I., et al. (2013). Somatic cells regulate maternal mRNA translation and developmental competence of mouse oocytes. Nat. Cell Biol. *15*, 1415–1423. https://doi.org/10.1038/ncb2873.
19. Wigglesworth, K., Lee, K.B., O'Brien, M.J., Peng, J., Matzuk, M.M., and Eppig, J.J. (2013). Bidirectional communication between oocytes and ovarian follicular somatic cells is required for meiotic arrest of mammalian oocytes. Proc. Natl. Acad. Sci. USA *110*, E3723–E3729. https://doi.org/10.1073/pnas.1314829110.
20. Horvath, S., and Raj, K. (2018). DNA methylation-based biomarkers and the epigenetic clock theory of ageing. Nat. Rev. Genet. *19*, 371–384. https://doi.org/10.1038/s41576-018-0004-3.
21. Levine, M.E., Lu, A.T., Quach, A., Chen, B.H., Assimes, T.L., Bandinelli, S., Hou, L., Baccarelli, A.A., Stewart, J.D., Li, Y., et al. (2018). An epigenetic biomarker of aging for lifespan and healthspan. Aging (Albany NY) *10*, 573–591. https://doi.org/10.18632/aging.101414.
22. Kordowitzki, P., Haghani, A., Zoller, J.A., Li, C.Z., Raj, K., Spangler, M.L., and Horvath, S. (2021). Epigenetic clock and methylation study of oocytes from a bovine model of reproductive aging. Aging Cell *20*, e13349. https://doi.org/10.1111/acel.13349.
23. Wu, M., Tang, W., Chen, Y., Xue, L., Dai, J., Li, Y., Zhu, X., Wu, C., Xiong, J., Zhang, J., et al. (2024). Spatiotemporal transcriptomic changes of human ovarian aging and the regulatory role of FOXP1. Nat. Aging *4*, 527–545. https://doi.org/10.1038/s43587-024-00607-1.
24. Ntostis, P., Iles, D., Kokkali, G., Vaxevanoglou, T., Kanavakis, E., Pantou, A., Huntriss, J., Pantos, K., and Picton, H.M. (2021). The impact of maternal age on gene expression during the GV to MII transition in

euploid human oocytes. Hum. Reprod. *37*, 80–92. https://doi.org/10.1093/humrep/deab226.

25. Zhang, J.J., Liu, X., Chen, L., Zhang, S., Zhang, X., Hao, C., and Miao, Y. L. (2020). Advanced maternal age alters expression of maternal effect genes that are essential for human oocyte quality. Aging (Albany NY) *12*, 3950–3961. https://doi.org/10.18632/aging.102864.
26. Qiao, J., Wang, Z.B., Feng, H.L., Miao, Y.L., Wang, Q., Yu, Y., Wei, Y.C., Yan, J., Wang, W.H., Shen, W., et al. (2014). The root of reduced fertility in aged women and possible therapentic options: current status and future perspects. Mol. Aspects Med. *38*, 54–85. https://doi.org/10.1016/j.mam.2013.06.001.
27. Miao, Y.L., Kikuchi, K., Sun, Q.Y., and Schatten, H. (2009). Oocyte aging: cellular and molecular changes, developmental potential and reversal possibility. Hum. Reprod. Update *15*, 573–585. https://doi.org/10.1093/humupd/dmp014.
28. Picelli, S., Faridani, O.R., Björklund, A.K., Winberg, G., Sagasser, S., and Sandberg, R. (2014). Full-length RNA-seq from single cells using Smart-seq2. Nat. Protoc. *9*, 171–181. https://doi.org/10.1038/nprot.2014.006.
29. Schober, P., Boer, C., and Schwarte, L.A. (2018). Correlation Coefficients: Appropriate Use and Interpretation. Anesth. Analg. *126*, 1763–1768. https://doi.org/10.1213/ANE.0000000000002864.
30. Smits, M.A.J., Janssens, G.E., Goddijn, M., Hamer, G., Houtkooper, R. H., and Mastenbroek, S. (2021). Longevity pathways are associated with human ovarian ageing. Hum. Reprod. Open *2021*, hoab020. https://doi.org/10.1093/hropen/hoab020.
31. Wang, X., Wang, L., and Xiang, W. (2023). Mechanisms of ovarian aging in women: a review. J. Ovarian Res. *16*, 67. https://doi.org/10.1186/s13048-023-01151-z.
32. Telfer, E.E., Grosbois, J., Odey, Y.L., Rosario, R., and Anderson, R.A. (2023). Making a good egg: human oocyte health, aging, and in vitro development. Physiol. Rev. *103*, 2623–2677. https://doi.org/10.1152/physrev.00032.2022.
33. Zhu, Z., Xu, W., and Liu, L. (2022). Ovarian aging: mechanisms and intervention strategies. Med. Rev. *2*, 590–610. https://doi.org/10.1515/mr-2022-0031.
34. Burdyniuk, M., Callegari, A., Mori, M., Nédélec, F., and Lénárt, P. (2018). F-Actin nucleated on chromosomes coordinates their capture by microtubules in oocyte meiosis. J. Cell Biol. *217*, 2661–2674. https://doi.org/10.1083/jcb.201802080.
35. Foltz, D.R., Jansen, L.E.T., Black, B.E., Bailey, A.O., Yates, J.R., 3rd, and Cleveland, D.W. (2006). The human CENP-A centromeric nucleosome-associated complex. Nat. Cell Biol. *8*, 458–469. https://doi.org/10.1038/ncb1397.
36. Hua, S., Wang, Z., Jiang, K., Huang, Y., Ward, T., Zhao, L., Dou, Z., and Yao, X. (2011). CENP-U cooperates with Hec1 to orchestrate kinetochore-microtubule attachment. J. Biol. Chem. *286*, 1627–1638. https://doi.org/10.1074/jbc.M110.174946.
37. Duncan, F.E., Hornick, J.E., Lampson, M.A., Schultz, R.M., Shea, L.D., and Woodruff, T.K. (2012). Chromosome cohesion decreases in human eggs with advanced maternal age. Aging Cell *11*, 1121–1124. https://doi.org/10.1111/j.1474-9726.2012.00866.x.
38. Buchwalter, A., and Hetzer, M.W. (2017). Nucleolar expansion and elevated protein translation in premature aging. Nat. Commun. *8*, 328. https://doi.org/10.1038/s41467-017-00322-z.
39. Duncan, F.E., Jasti, S., Paulson, A., Kelsh, J.M., Fegley, B., and Gerton, J.L. (2017). Age-associated dysregulation of protein metabolism in the mammalian oocyte. Aging Cell *16*, 1381–1393. https://doi.org/10.1111/acel.12676.
40. Liu, G.Y., and Sabatini, D.M. (2020). mTOR at the nexus of nutrition, growth, ageing and disease. Nat. Rev. Mol. Cell Biol. *21*, 183–203. https://doi.org/10.1038/s41580-019-0199-y.
41. Green, C.L., Lamming, D.W., and Fontana, L. (2022). Molecular mechanisms of dietary restriction promoting health and longevity. Nat. Rev. Mol. Cell Biol. *23*, 56–73. https://doi.org/10.1038/s41580-021-00411-4.
42. Shen, D., Coleman, J., Chan, E., Nicholson, T.P., Dai, L., Sheppard, P.W., and Patton, W.F. (2011). Novel cell- and tissue-based assays for detecting misfolded and aggregated protein accumulation within aggresomes and inclusion bodies. Cell Biochem. Biophys. *60*, 173–185. https://doi.org/10.1007/s12013-010-9138-4.
43. Horvath, S. (2013). DNA methylation age of human tissues and cell types. Genome Biol. *14*, R115. https://doi.org/10.1186/gb-2013-14-10-r115.
44. Morin, S.J., Tao, X., Marin, D., Zhan, Y., Landis, J., Bedard, J., Scott, R. T., and Seli, E. (2018). DNA methylation-based age prediction and telomere length in white blood cells and cumulus cells of infertile women with normal or poor response to ovarian stimulation. Aging (Albany NY) *10*, 3761–3773. https://doi.org/10.18632/aging.101670.
45. Yu, C., Zhang, Y.L., Pan, W.W., Li, X.M., Wang, Z.W., Ge, Z.J., Zhou, J.J., Cang, Y., Tong, C., Sun, Q.Y., and Fan, H.Y. (2013). CRL4 complex regulates mammalian oocyte survival and reprogramming by activation of TET proteins. Science *342*, 1518–1521. https://doi.org/10.1126/science.1244587.
46. Percharde, M., Lin, C.J., Yin, Y., Guan, J., Peixoto, G.A., Bulut-Karslioglu, A., Biechele, S., Huang, B., Shen, X., and Ramalho-Santos, M. (2018). A LINE1-Nucleolin Partnership Regulates Early Development and ESC Identity. Cell *174*, 391–405.e19. https://doi.org/10.1016/j.cell.2018.05.043.
47. Zhang, W., Qu, J., Liu, G.H., and Belmonte, J.C.I. (2020). The ageing epigenome and its rejuvenation. Nat. Rev. Mol. Cell Biol. *21*, 137–150. https://doi.org/10.1038/s41580-019-0204-5.
48. Wasserzug-Pash, P., Rothman, R., Reich, E., Zecharyahu, L., Schonberger, O., Weiss, Y., Srebnik, N., Cohen-Hadad, Y., Weintraub, A., Ben-Ami, I., et al. (2022). Loss of heterochromatin and retrotransposon silencing as determinants in oocyte aging. Aging Cell *21*, e13568. https://doi.org/10.1111/acel.13568.
49. Zhang, W., Li, J., Suzuki, K., Qu, J., Wang, P., Zhou, J., Liu, X., Ren, R., Xu, X., Ocampo, A., et al. (2015). Aging stem cells. A Werner syndrome stem cell model unveils heterochromatin alterations as a driver of human aging. Science *348*, 1160–1163. https://doi.org/10.1126/science.aaa1356.
50. Xin, D.E., Liao, Y., Rao, R., Ogurek, S., Sengupta, S., Xin, M., Bayat, A.E., Seibel, W.L., Graham, R.T., Koschmann, C., and Lu, Q.R. (2024). Chaetocin-mediated SUV39H1 inhibition targets stemness and oncogenic networks of diffuse midline gliomas and synergizes with ONC201. Neuro Oncol. *26*, 735–748. https://doi.org/10.1093/neuonc/noad222.
51. Kraig, E., Linehan, L.A., Liang, H., Romo, T.Q., Liu, Q., Wu, Y., Benavides, A.D., Curiel, T.J., Javors, M.A., Musi, N., et al. (2018). A randomized control trial to establish the feasibility and safety of rapamycin treatment in an older human cohort: Immunological, physical performance, and cognitive effects. Exp. Gerontol. *105*, 53–69. https://doi.org/10.1016/j.exger.2017.12.026.
52. Singh, M., Jensen, M.D., Lerman, A., Kushwaha, S., Rihal, C.S., Gersh, B. J., Behfar, A., Tchkonia, T., Thomas, R.J., Lennon, R.J., et al. (2016). Effect of Low-Dose Rapamycin on Senescence Markers and Physical Functioning in Older Adults with Coronary Artery Disease: Results of a Pilot Study. J. Frailty Aging *5*, 204–207. https://doi.org/10.14283/jfa.2016.112.
53. Vuong, L.N., Dang, V.Q., Ho, T.M., Huynh, B.G., Ha, D.T., Pham, T.D., Nguyen, L.K., Norman, R.J., and Mol, B.W. (2018). IVF Transfer of Fresh or Frozen Embryos in Women without Polycystic Ovaries. N. Engl. J. Med. *378*, 137–147. https://doi.org/10.1056/NEJMoa1703768.
54. Alpha Scientists in Reproductive Medicine and ESHRE Special Interest Group of Embryology (2011). The Istanbul consensus workshop on embryo assessment: proceedings of an expert meeting. Hum. Reprod. *26*, 1270–1283. https://doi.org/10.1093/humrep/der037.

55. Papanikolaou, E.G., Camus, M., Kolibianakis, E.M., Van Landuyt, L., Van Steirteghem, A., and Devroey, P. (2006). In vitro fertilization with single blastocyst-stage versus single cleavage-stage embryos. N. Engl. J. Med. *354*, 1139–1146. https://doi.org/10.1056/NEJMoa053524.

56. Schoolcraft, W.B., Gardner, D.K., Lane, M., Schlenker, T., Hamilton, F., and Meldrum, D.R. (1999). Blastocyst culture and transfer: analysis of results and parameters affecting outcome in two in vitro fertilization programs. Fertil. Steril. *72*, 604–609. https://doi.org/10.1016/s0015-0282(99)00311-8.

57. Plancha, C.E., Sanfins, A., Rodrigues, P., and Albertini, D. (2005). Cell polarity during folliculogenesis and oogenesis. Reprod. Biomed. Online *10*, 478–484. https://doi.org/10.1016/s1472-6483(10)60824-3.

58. Gilchrist, R.B., Lane, M., and Thompson, J.G. (2008). Oocyte-secreted factors: regulators of cumulus cell function and oocyte quality. Hum. Reprod. Update *14*, 159–177. https://doi.org/10.1093/humupd/dmm040.

59. Li, H.Y., Wang, M., Jiang, X., Jing, Y., Wu, Z., He, Y., Yan, K., Sun, S., Ma, S., Ji, Z., et al. (2024). CRISPR screening uncovers nucleolar RPL22 as a heterochromatin destabilizer and senescence driver. Nucleic Acids Res. *52*, 11481–11499. https://doi.org/10.1093/nar/gkae740.

60. Hirai, H., Sen, Y., Tamura, M., and Ohta, K. (2023). TOR inactivation triggers heterochromatin formation in rDNA during glucose starvation. Cell Rep. *42*, 113320. https://doi.org/10.1016/j.celrep.2023.113320.

61. Sun, D., Luo, M., Jeong, M., Rodriguez, B., Xia, Z., Hannah, R., Wang, H., Le, T., Faull, K.F., Chen, R., et al. (2014). Epigenomic profiling of young and aged HSCs reveals concerted changes during aging that reinforce self-renewal. Cell Stem Cell *14*, 673–688. https://doi.org/10.1016/j.stem.2014.03.002.

62. Holubcova, Z., Blayney, M., Elder, K., and Schuh, M. (2015). Human oocytes. Error-prone chromosome-mediated spindle assembly favors chromosome segregation defects in human oocytes. Science *348*, 1143–1147. https://doi.org/10.1126/science.aaa9529.

63. So, C., Menelaou, K., Uraji, J., Harasimov, K., Steyer, A.M., Seres, K.B., Bucevičius, J., Lukinavičius, G., Möbius, W., Sibold, C., et al. (2022). Mechanism of spindle pole organization and instability in human oocytes. Science *375*, eabj3944. https://doi.org/10.1126/science.abj3944.

64. Mogessie, B., and Schuh, M. (2017). Actin protects mammalian eggs against chromosome segregation errors. Science *357*, eaal1647. https://doi.org/10.1126/science.aal1647.

65. Wu, T., Dong, J., Fu, J., Kuang, Y., Chen, B., Gu, H., Luo, Y., Gu, R., Zhang, M., Li, W., et al. (2022). The mechanism of acentrosomal spindle assembly in human oocytes. Science *378*, eabq7361. https://doi.org/10.1126/science.abq7361.

66. Harasimov, K., Gorry, R.L., Welp, L.M., Penir, S.M., Horokhovskyi, Y., Cheng, S., Takaoka, K., Stützer, A., Frombach, A.S., Taylor Tavares, A.L., et al. (2024). The maintenance of oocytes in the mammalian ovary involves extreme protein longevity. Nat. Cell Biol. *26*, 1124–1138. https://doi.org/10.1038/s41556-024-01442-7.

67. Stein, K.C., Morales-Polanco, F., van der Lienden, J., Rainbolt, T.K., and Frydman, J. (2022). Ageing exacerbates ribosome pausing to disrupt cotranslational proteostasis. Nature *601*, 637–642. https://doi.org/10.1038/s41586-021-04295-4.

68. Leesch, F., Lorenzo-Orts, L., Pribitzer, C., Grishkovskaya, I., Roehsner, J., Chugunova, A., Matzinger, M., Roitinger, E., Belačić, K., Kandolf, S., et al. (2023). A molecular network of conserved factors keeps ribosomes dormant in the egg. Nature *613*, 712–720. https://doi.org/10.1038/s41586-022-05623-y.

69. Xiao, F.H., Yu, Q., Deng, Z.L., Yang, K., Ye, Y., Ge, M.X., Yan, D., Wang, H.T., Chen, X.Q., Yang, L.Q., et al. (2022). ETS1 acts as a regulator of human healthy aging via decreasing ribosomal activity. Sci. Adv. *8*, eabf2017. https://doi.org/10.1126/sciadv.abf2017.

70. Bolger, A.M., Lohse, M., and Usadel, B. (2014). Trimmomatic: a flexible trimmer for Illumina sequence data. Bioinformatics *30*, 2114–2120. https://doi.org/10.1093/bioinformatics/btu170.

71. Kim, D., Langmead, B., and Salzberg, S.L. (2015). HISAT: a fast spliced aligner with low memory requirements. Nat. Methods *12*, 357–360. https://doi.org/10.1038/nmeth.3317.

72. Liao, Y., Smyth, G.K., and Shi, W. (2014). featureCounts: an efficient general purpose program for assigning sequence reads to genomic features. Bioinformatics *30*, 923–930. https://doi.org/10.1093/bioinformatics/btt656.

73. Huang, D.W., Sherman, B.T., and Lempicki, R.A. (2009). Systematic and integrative analysis of large gene lists using DAVID bioinformatics resources. Nat. Protoc. *4*, 44–57. https://doi.org/10.1038/nprot.2008.211.

74. Shannon, P., Markiel, A., Ozier, O., Baliga, N.S., Wang, J.T., Ramage, D., Amin, N., Schwikowski, B., and Ideker, T. (2003). Cytoscape: a software environment for integrated models of biomolecular interaction networks. Genome Res. *13*, 2498–2504. https://doi.org/10.1101/gr.1239303.

75. Subramanian, A., Tamayo, P., Mootha, V.K., Mukherjee, S., Ebert, B.L., Gillette, M.A., Paulovich, A., Pomeroy, S.L., Golub, T.R., Lander, E.S., and Mesirov, J.P. (2005). Gene set enrichment analysis: a knowledge-based approach for interpreting genome-wide expression profiles. Proc. Natl. Acad. Sci. USA *102*, 15545–15550. https://doi.org/10.1073/pnas.0506580102.

76. Krueger, F., and Andrews, S.R. (2011). Bismark: a flexible aligner and methylation caller for Bisulfite-Seq applications. Bioinformatics *27*, 1571–1572. https://doi.org/10.1093/bioinformatics/btr167.

77. Akalin, A., Kormaksson, M., Li, S., Garrett-Bakelman, F.E., Figueroa, M.E., Melnick, A., and Mason, C.E. (2012). methylKit: a comprehensive R package for the analysis of genome-wide DNA methylation profiles. Genome Biol. *13*, R87. https://doi.org/10.1186/gb-2012-13-10-r87.

78. Love, M.I., Huber, W., and Anders, S. (2014). Moderated estimation of fold change and dispersion for RNA-seq data with DESeq2. Genome Biol. *15*, 550. https://doi.org/10.1186/s13059-014-0550-8.

79. Langmead, B., and Salzberg, S.L. (2012). Fast gapped-read alignment with Bowtie 2. Nat. Methods *9*, 357–359. https://doi.org/10.1038/nmeth.1923.

80. Zhang, Y., Liu, T., Meyer, C.A., Eeckhoute, J., Johnson, D.S., Bernstein, B.E., Nusbaum, C., Myers, R.M., Brown, M., Li, W., and Liu, X.S. (2008). Model-based analysis of ChIP-Seq (MACS). Genome Biol. *9*, R137. https://doi.org/10.1186/gb-2008-9-9-r137.

81. Yu, G., Wang, L.G., and He, Q.Y. (2015). ChIPseeker: an R/Bioconductor package for ChIP peak annotation, comparison and visualization. Bioinformatics *31*, 2382–2383. https://doi.org/10.1093/bioinformatics/btv145.

82. Ramirez, F., Ryan, D.P., Gruning, B., Bhardwaj, V., Kilpert, F., Richter, A.S., Heyne, S., Dundar, F., and Manke, T. (2016). deepTools2: a next generation web server for deep-sequencing data analysis. Nucleic Acids Res. *44*, W160–W165. https://doi.org/10.1093/nar/gkw257.

83. Tian, C., Liu, L., Ye, X., Fu, H., Sheng, X., Wang, L., Wang, H., Heng, D., and Liu, L. (2019). Functional Oocytes Derived from Granulosa Cells. Cell Rep. *29*, 4256–4267.e9. https://doi.org/10.1016/j.celrep.2019.11.080.

84. Chen, Z.J., Shi, Y., Sun, Y., Zhang, B., Liang, X., Cao, Y., Yang, J., Liu, J., Wei, D., Weng, N., et al. (2016). Fresh versus Frozen Embryos for Infertility in the Polycystic Ovary Syndrome. N. Engl. J. Med. *375*, 523–533. https://doi.org/10.1056/NEJMoa1513873.

85. Haouzi, D., Assou, S., Monzo, C., Vincens, C., Dechaud, H., and Hamamah, S. (2012). Altered gene expression profile in cumulus cells of mature MII oocytes from patients with polycystic ovary syndrome. Hum. Reprod. *27*, 3523–3530. https://doi.org/10.1093/humrep/des325.

86. Xu, W., Li, L., Sun, J., Zhu, S., Yan, Z., Gao, L., Gao, C., Cui, Y., and Mao, C. (2018). Putrescine delays postovulatory aging of mouse oocytes by upregulating PDK4 expression and improving mitochondrial activity. Aging (Albany NY) *10*, 4093–4106. https://doi.org/10.18632/aging.101699.

87. Allworth, A.E., and Albertini, D.F. (1993). Meiotic maturation in cultured bovine oocytes is accompanied by remodeling of the cumulus

cell cytoskeleton. Dev. Biol. *158*, 101–112. https://doi.org/10.1006/dbio.1993.1171.

88. Haakonsen, D.L., Heider, M., Ingersoll, A.J., Vodehnal, K., Witus, S.R., Uenaka, T., Wernig, M., and Rapé, M. (2024). Stress response silencing by an E3 ligase mutated in neurodegeneration. Nature *626*, 874–880. https://doi.org/10.1038/s41586-023-06985-7.

89. Zhang, M., Wang, Z., Zhao, Q., Yang, Q., Bai, J., Yang, C., Zhang, Z.R., and Liu, Y. (2024). USP20 deubiquitinates and stabilizes the reticulophagy receptor RETREG1/FAM134B to drive reticulophagy. Autophagy *20*, 1780–1797. https://doi.org/10.1080/15548627.2024.2347103.

90. Ketola, K., Kaljunen, H., Taavitsainen, S., Kaarijärvi, R., Järvelä, E., Rodríguez-Martín, B., Haase, K., Woodcock, D.J., Tubio, J., Wedge, D.C., et al. (2021). Subclone Eradication Analysis Identifies Targets for Enhanced Cancer Therapy and Reveals L1 Retrotransposition as a Dynamic Source of Cancer Heterogeneity. Cancer Res. *81*, 4901–4909. https://doi.org/10.1158/0008-5472.CAN-21-0371.

91. Wang, R., Yu, Z., Sunchu, B., Shoaf, J., Dang, I., Zhao, S., Caples, K., Bradley, L., Beaver, L.M., Ho, E., et al. (2017). Rapamycin inhibits the secretory phenotype of senescent cells by a Nrf2-independent mechanism. Aging Cell *16*, 564–574. https://doi.org/10.1111/acel.12587.

92. Deng, X., Zhang, X., Li, W., Feng, R.X., Li, L., Yi, G.R., Zhang, X.N., Yin, C., Yu, H.Y., Zhang, J.P., et al. (2018). Chronic Liver Injury Induces Conversion of Biliary Epithelial Cells into Hepatocytes. Cell Stem Cell *23*, 114–122.e3. https://doi.org/10.1016/j.stem.2018.05.022.

93. Wang, H., Zhang, K., Liu, Y., Fu, Y., Gao, S., Gong, P., Wang, H., Zhou, Z., Zeng, M., Wu, Z., et al. (2017). Telomere heterogeneity linked to metabolism and pluripotency state revealed by simultaneous analysis of telomere length and RNA-seq in the same human embryonic stem cell. BMC Biol. *15*, 114. https://doi.org/10.1186/s12915-017-0453-8.

94. Smallwood, S.A., Lee, H.J., Angermueller, C., Krueger, F., Saadeh, H., Peat, J., Andrews, S.R., Stegle, O., Reik, W., and Kelsey, G. (2014). Single-cell genome-wide bisulfite sequencing for assessing epigenetic heterogeneity. Nat. Methods *11*, 817–820. https://doi.org/10.1038/nmeth.3035.

95. Kaya-Okur, H.S., Wu, S.J., Codomo, C.A., Pledger, E.S., Bryson, T.D., Henikoff, J.G., Ahmad, K., and Henikoff, S. (2019). CUT&Tag for efficient epigenomic profiling of small samples and single cells. Nat. Commun. *10*, 1930. https://doi.org/10.1038/s41467-019-09982-5.

96. Jin, Y., Tam, O.H., Paniagua, E., and Hammell, M. (2015). TEtranscripts: a package for including transposable elements in differential expression analysis of RNA-seq datasets. Bioinformatics *31*, 3593–3599. https://doi.org/10.1093/bioinformatics/btv422.

97. Ohtani, H., Liu, M., Zhou, W., Liang, G., and Jones, P.A. (2018). Switching roles for DNA and histone methylation depend on evolutionary ages of human endogenous retroviruses. Genome Res. *28*, 1147–1157. https://doi.org/10.1101/gr.234229.118.

98. Dahlet, T., Argüeso Lleida, A., Al Adhami, H., Dumas, M., Bender, A., Ngondo, R.P., Tanguy, M., Vallet, J., Auclair, G., Bardet, A.F., and Weber, M. (2020). Genome-wide analysis in the mouse embryo reveals the importance of DNA methylation for transcription integrity. Nat. Commun. *11*, 3153. https://doi.org/10.1038/s41467-020-16919-w.

99. Wang, L., Zhang, J., Duan, J., Gao, X., Zhu, W., Lu, X., Yang, L., Zhang, J., Li, G., Ci, W., et al. (2014). Programming and inheritance of parental DNA methylomes in mammals. Cell *157*, 979–991. https://doi.org/10.1016/j.cell.2014.04.017.

100. Wang, H.Q., Tuominen, L.K., and Tsai, C.J. (2011). SLIM: a sliding linear model for estimating the proportion of true null hypotheses in datasets with dependence structures. Bioinformatics *27*, 225–231. https://doi.org/10.1093/bioinformatics/btq650.

101. Delacher, M., Imbusch, C.D., Weichenhan, D., Breiling, A., Hotz-Wagenblatt, A., Träger, U., Hofer, A.C., Kägebein, D., Wang, Q., Frauhammer, F., et al. (2017). Genome-wide DNA-methylation landscape defines specialization of regulatory T cells in tissues. Nat. Immunol. *18*, 1160–1172. https://doi.org/10.1038/ni.3799.

102. Heinz, S., Benner, C., Spann, N., Bertolino, E., Lin, Y.C., Laslo, P., Cheng, J.X., Murre, C., Singh, H., and Glass, C.K. (2010). Simple combinations of lineage-determining transcription factors prime cis-regulatory elements required for macrophage and B cell identities. Mol. Cell *38*, 576–589. https://doi.org/10.1016/j.molcel.2010.05.004.

103. Hochberg, Y., and Benjamini, Y. (1990). More powerful procedures for multiple significance testing. Stat. Med. *9*, 811–818. https://doi.org/10.1002/sim.4780090710.

104. Yu, H., Chen, M., Hu, Y., Ou, S., Yu, X., Liang, S., Li, N., Yang, M., Kong, X., Sun, C., et al. (2022). Dynamic reprogramming of H3K9me3 at hominoid-specific retrotransposons during human preimplantation development. Cell Stem Cell *29*, 1031–1050.e12. https://doi.org/10.1016/j.stem.2022.06.006.

105. McLean, C.Y., Bristor, D., Hiller, M., Clarke, S.L., Schaar, B.T., Lowe, C.B., Wenger, A.M., and Bejerano, G. (2010). GREAT improves functional interpretation of cis-regulatory regions. Nat. Biotechnol. *28*, 495–501. https://doi.org/10.1038/nbt.1630.

STAR★METHODS

KEY RESOURCES TABLE

REAGENT or RESOURCE	SOURCE	IDENTIFIER
Antibodies		
H3K9me3	Abcam	Cat#ab8898; RRID: AB_306848
H3K27me3	Millipore	Cat#07–449; RRID: AB_310624
53BP1	Abcam	Cat#ab36823; RRID: AB_722497
LINE-1 ORF1p	Millipore	Cat#MABC1152; RRID: AB_2941775
Rabbit monoclonal anti-Phospho-S6 Ribosomal Protein (Ser235/S236)	Cell Signaling Technology	Cat#4858S; RRID: AB_916156
Rabbit monoclonal anti-S6 Ribosomal Protein (5G10)	Cell Signaling Technology	Cat#2217S; RRID: AB_331355
anti-β-Actin	ABclonal	Cat#AC026; RRID: AB_2768234
4E-BP1	Cell Signaling Technology	Cat#9644T; RRID: AB_2097841
Phospho-4E-BP1 (Ser65)	Cell Signaling Technology	Cat#9451T; RRID: AB_330947
mTOR	Cell Signaling Technology	Cat#2983S; RRID: AB_2105622
Phospho-mTOR (Ser2448)	Cell Signaling Technology	Cat#5536T; RRID: AB_10691552
alpha-Tubulin-FITC	Sigma-Aldrich	Cat#F2168; RRID: AB_476967
Nucleolin	Cell Signaling Technology	Cat#14574S; RRID: AB_2798519
Donkey anti-rabbit IgG Alexa Fluor 594 antibody	Thermo Scientific	Cat#A-21207; RRID: AB_141637
Donkey anti-mouse IgG Alexa Fluor 488 antibody	Thermo Scientific	Cat#A-21202; RRID: AB_141607
Biological samples		
Female oocytes	Patient donators in this study	N/A
Female cumulus cells	Patient donators in this study	N/A
Chemicals, peptides, and recombinant proteins		
Hyaluronidase	Sigma-Aldrich	Cat#H6254-500MG
Polyvinylpyrrolidone	Sigma-Aldrich	Cat#P0930-50G
Tyrode's Acidic Solution	Sigma-Aldrich	Cat#T1788-100ML
DMEM NUTRIENT MIX F12	Thermo Scientific	Cat#11330032
Hoechst 33342	Thermo Scientific	Cat#H3570
MG132	MCE	Cat#HY-13259
Bafilomycin A	Selleck	Cat#S1413
Chaetocin	MCE	Cat#HY-N2019
LysoTracker red	Beyotime	Cat#C1046
Azidothymidine	Sigma-Aldrich	Cat#A2169
Chemiluminescent HRP substrate	Millipore	Cat#WBKLS0500
PVDF membranes	Millipore	Cat#ISEQ00010
FastStart Universal SYBR Green Master Mix	Roche	Cat#4913914001
M-MLV Reverse Transcriptase	Invitrogen	Cat#28025-021
Agencourt Ampure XP beads	Beckman	Cat#A63881
M-280 Streptavidin Dynabeads	Life Technologies	Cat#65001
KAPA HiFi HotStart DNA Polymerase	KAPA Biosystems	Cat#KK2801
Spermidine	MCE	Cat#HY-B1776
Roche Complete Protease Inhibitor EDTA-Free tablets	Sigma-Aldrich	Cat#5056489001
Critical commercial assays		
Senescence-associated β-galactosidase staining kit	Beyotime	Cat#C0602
RNeasy RNA Micro Kit	QIAGEN	Cat#74034

(*Continued on next page*)

Continued		
REAGENT or RESOURCE	SOURCE	IDENTIFIER
PROTEOSTAT® Aggresome detection kit	Enzo Life Sciences	Cat#ENZ-51035-K25
TruePrep DNA Library Prep Kit V2 for Illumina®	Vazyme Biotech	Cat#TD503-02
QIAamp® DNA Micro Kit	QIAGEN	Cat#56304
BeyoClick™ HPG-594 Protein Synthesis Assay Kit	Beyotime	Cat#P1209S
Deposited data		
The raw RNA-seq data for female oocytes and cumulus cells	This paper	NGDC: HRA005257
The raw MethylC-Seq data for female oocytes and cumulus cells	This paper	NGDC: HRA005257
The raw CUT&Tag data for female cumulus cells	This paper	NGDC: HRA005257
Oligonucleotides		
Primers for qRT-PCR, see Table S7	This paper	N/A
Software and algorithms		
Trimmomatic (v0.38)	Bolger et al.[70]	http://www.usadellab.org/cms/index.php?page=trimmomatic
hisat2 (v2.1.0)	Kim et al.[71]	https://ccb.jhu.edu/software/hisat2/index.shtml
featureCounts (v1.6.3)	Liao et al.[72]	http://subread.sourceforge.net/
R (v4.4.1)	CRAN	https://www.r-project.org/
DAVID (v6.8)	Huang et al.[73]	https://david.ncifcrf.gov
Cytoscape (v3.9.1)	Shannon et al.[74]	https://cytoscape.org
GSEA (v4.3.3)	Subramanian et al.[75]	https://www.gsea-msigdb.org/gsea/index.jsp
Bismark (v0.19.1)	Krueger et al.[76]	http://www.bioinformatics.babraham.ac.uk/projects/bismark/
MethylKit (1.30.0)	Akalin et al.[77]	https://www.bioconductor.org/packages/release/bioc/html/methylKit.html
DESeq2 (v1.44.0)	Love et al.[78]	https://www.bioconductor.org/packages/release/bioc/html/DESeq2.html
Bowtie2 (v2.3.4)	Langmead et al.[79]	http://bowtie-bio.sourceforge.net/bowtie2/index.shtml
macs2 (v2.1.2)	Zhang et al.[80]	https://pypi.org/project/MACS2/
ChIPseeker (v1.28.3)	Yu et al.[81]	https://guangchuangyu.github.io/software/ChIPseeker/
deepTools (v3.2.0)	Ramirez et al.[82]	https://deeptools.readthedocs.io/en/develop/
SPSS Statistics (v29.0.0)	IBM	https://www.ibm.com/spss
ImageJ	NIH	https://imagej.nih.gov/ij/
Prism (v8.4.3)	GraphPad Software	https://www.graphpad.com/

EXPERIMENTAL MODEL AND STUDY PARTICIPANT DETAILS

Mice and housing conditions

Young (2-month-old) and old (10-month-old) female C57BL/6 background mice were purchased from Beijing Vital River Laboratory Animal Technology Co., Ltd. All the mice were cared for in individually ventilated cages (IVCs) on a standard 12 h:12 h dark cycle in the sterile animal facility at the College of Life Sciences. The mice used in this study were approved by the Nankai University Animal Care and Use Committee, and all mouse experiments were carried out in accordance with the guidelines and relevant regulations.

Mouse cumulus cells and culture

Isolation of mouse cumulus cells (mCCs) and culture were performed as previously described.[83] Briefly, PMSG was injected into the abdominal cavity of mice 46 h before the mCCs were isolated. The mice were humanely sacrificed, and the ovaries were dissected. Insulin syringes were used to puncture visible follicles on the surface of the ovaries under a stereomicroscope to release mCCs into the culture medium, avoiding isolation of mCCs from small follicles. In addition, the oocytes were filtered out via a 40-μm cell strainer (Falcon). The isolated mCCs were subsequently washed three times and seeded in culture medium.

Ethics statement

This study was approved by the Ethics Committee of TianJin Medical University General Hospital (No: IRB2018-102-01), the Sixth Medical Center of Chinese People's Liberation Army (PLA) General Hospital (No: HZKY-PJ-2021-33), Shanxi Medical University (No. 2022SJL75) and Amcare Women's & Children's Hospital (No: AM2020-001-01; AM-2024001) and was conducted in accordance with approved institutional guidelines. Written informed consent was obtained from the donors.

Human subjects

The isolated oocytes and surrounding CC samples were obtained from 100 female donors ranging in age from 23 to 48 years. The inclusion criteria for donors undergoing IVF/ICSI with their own oocytes included maternal age and male factor infertility, and donors were excluded from the study if they had endometriosis, cancer, chronic infections, or autoimmune or genetic diseases. The mean ovarian reserve was 18 (range 3–55), which was represented by the antral follicle count (AFC) obtained from donors whose clinical samples were used for RNA-seq and MethylC-seq. The clinical characteristics of all donors, including cell type and age, were collected and are summarized in Table S1.

Clinical study design and oversight

We conducted a randomized, controlled trial at the Children's Hospital of Shanxi and Women's Health Center of Shanxi. The study was approved by the Ethics Committee of Shanxi Medical University (ethics number: 2022SJL75) and conducted according to the Declaration of Helsinki 2013, and the trial was registered at the Chinese Clinical Trial Registry (https://www.chictr.org.cn/) with registration number (ChiCTR2300069828). Independent data and safety monitoring boards were established to oversee the study. All patients provided written informed consent before participation. From April 2023, a total of 122 patients underwent screening, and 100 patients met the eligibility criteria and were enrolled in the study.

Clinical study: Inclusion and exclusion criteria

The study included infertile women who had a history of more than one IVF cycle failure and who provided informed consent. The average age of all the women was approximately 36 years. The exclusion criteria included patients with infertility due to male factors such as oligozoospermia or azoospermia, and patients with sexually transmitted diseases, genetic diseases, uterine malformations and a history of endometriotic cyst surgery. Patients with allergies to rapamycin and its derivatives and other serious systemic diseases were excluded.

Clinical study: Sample size estimation

Referring to a published clinical trial article,[84] *a priori* power analysis was conducted to determine the sample size required to detect statistically significant changes associated with the clinical pregnancy rate. The study was designed to have a power of 80% at a two-sided significance level (α) of 0.05 to detect an absolute difference of 30 percentage points in the clinical pregnancy rate between the two groups (clinical pregnancy rate of 30% for the control group and 60% for the rapamycin group) by means of Pearson's chi-square test. At least 42 patients per study group were needed, a number that we increased to 50 to allow for a dropout rate of 10% (Details are provided in Data S1).

IVF-ET procedures

The patients were randomly assigned to one of the two study groups (the control and rapamycin groups) at a 1:1 ratio, and the statisticians used SPSS statistical software to generate random numbers. The odd numbers were assigned to the rapamycin group, and the even numbers were assigned to the control group. The random numbers and grouping information were prepacked in the envelope, which was unknown to the clinical investigators. When the subjects were enrolled in the group, the envelopes were opened in sequence and grouped according to the groups in the envelopes.

All patients received a standardized long GnRH agonist protocol, oocyte retrieval, fertilization, and planned embryo transfer. In brief, in the mid-luteal phase of the previous menstrual cycle, 0.1 mg of triptorelin acetate (triptorelin) was used for downregulation for 14–16 days. On the 2nd to 5th days of the menstrual cycle, the serum hormone levels (FSH, LH, and E2) and ultrasonography results were monitored. Gonadotropin (Gn) was used after the downregulation standard was reached (FSH $\leq$5 mIU/mL, LH $\leq$ 5 mIU/mL, E2 $\leq$ 50 pg/mL). Gonadotropin (Gn) was given at 75–300 IU. The Gn dose was adjusted according to the growth of the follicle and the hormone levels. When more than one follicle with a diameter greater than 18 mm appeared, intramuscular injection of human chorionic gonadotropin (hCG) 6000–10000 IU was given. Oocyte retrieval was performed 36 h later.

The obtained oocytes were inseminated approximately 4–6 h by a conventional method or intracytoplasmic sperm injection according to the sperm quality, and a fertilization check was then performed 16 to 18 h after insemination. The embryos were scored according to the morphological criteria.[54] The quality of the blastocysts was assessed according to the criteria of Gardner and Schoolcraft.[56] High-quality embryos on day 3 or blastocysts on days 5–6 were selected for fresh transfer or cryopreserved via vitrification and frozen-embryo transfer. Transfer on day 3 or days 5–6 depends on the quality of the embryo and the patient's wishes. When more embryos were high quality on day 3 and the probability of achieving high-quality blastocysts at days 5–6 was high, the patients were persuaded to choose continuous cultures to obtain 5–6 blastocysts for embryo transfer. Otherwise, the patients were suggested to choose embryo transfer immediately without attempting further culture to obtain blastocysts. Luteal-phase support

was administered before embryo transfer and continued until 10 weeks of gestation. Biochemical pregnancy was defined as a human chorionic gonadotropin level of more than 10 mIU per milliliter, as measured at 10 days after embryo transfer. Clinical pregnancy was defined as the presence of a gestational sac in the uterine cavity at 30 days after embryo transfer, as detected by ultrasonography. Live birth was defined as the delivery of a live-born infant around the due date of pregnancy.[84]

Clinical interventions

The dosage and duration of rapamycin were determined according to previous articles and registered clinical trials.[51,52] For patients in the rapamycin group, oral rapamycin (sirolimus, Rapamune; Pfizer) at a daily dose of 1 mg was administered for 21–28 days beginning on the day of endogenous hormone downregulation until oocyte retrieval, which was defined as short-term use.

Clinical outcomes

The primary outcomes were oocyte number and embryo number. The secondary outcome was the rate of clinical pregnancy.

Ovarian stimulation

All donors underwent controlled ovarian stimulation. An ultrasound scan and serum estradiol assays were performed to monitor follicular size, which ensured that the cumulus–oocyte complexes obtained from comparable follicles of the same developmental stage. When two or more follicles were at least 12 mm in diameter, 10,000 IU human chorionic gonadotropin (hCG) was administered 36 h before oocyte retrieval.

Oocyte retrieval and isolation of cumulus cells

The cumulus–oocyte complex (COC) was isolated via ultrasound-guided vaginal puncture and classified according to the oocyte nuclear maturation stage: GV (germinal vesicle), MI (metaphase I) and MII (metaphase II). We collected only GV-stage oocytes and surrounding CCs for this study, whereas MII-stage oocytes were used for clinical fertilization.

The CCs were collected as previously described.[85] Briefly, CCs were mechanically stripped from oocytes under stereomicroscopy, and then, the isolated CCs were dispersed into single cells with 0.03% hyaluronidase (H6254-500MG, Sigma–Aldrich) and resuspended three times in PBS. The separated CCs were counted as up to 500 cells and placed in the lysate. Tyrode's acidic solution (T1788-100ML, Sigma–Aldrich) was used to facilitate stripping of the zona pellucida to produce naked oocytes. Oocytes were observed under a microscope to ensure the absence of contamination with CCs. Naked oocytes were carefully washed three times with PBS containing 0.1% polyvinylpyrrolidone (PVP, P0930-50G, Sigma–Aldrich) to prevent them from adhering to tools or dishes and then placed in lysis buffer.

Human cumulus cells and culture

Human cumulus cells were dissected from the GV-stage cumulus–oocyte complex (COC) and purified from Amcare Women's & Children's Hospital. Briefly, cumulus cells were mechanically stripped from oocytes under stereomicroscopy and then dispersed into single cells with 0.03% hyaluronidase. Next, the cells were suspended in 1 mL of medium containing DMEM/F12 supplemented with 10% FBS and 1% penicillin–streptomycin and centrifuged again. Next, the supernatant was decanted, and the cell pellet was resuspended in fresh medium and plated. The cells were cultured for three days at 37°C in a 5% CO_2 incubator. Young and old CC samples were taken from the same day and cultured for the same number of days in each batch of experiments.

METHOD DETAILS

In vitro maturation of mouse oocytes

At 2 and 10 months of age, female mice were humanely sacrificed after PMSG injection at 44–46 h intervals. After the ovaries were dissected, fully grown germinal vesicle (GV) oocytes were collected under a microscope by pricking the follicles in IVM medium (α-MEM with 5% fetal bovine serum (FBS), 0.24 mM sodium pyruvate, 1 IU/mL PMSG, and 1.5 IU/mL hCG) via an insulin syringe. The obtained GV oocytes were divided into two equal parts and then placed in IVM medium (with or without rapamycin). Oocytes were matured in IVM medium for 17–18 h at 37°C. MII oocytes were determined by extrusion of the first polar body.

ROS assay

2′,7′-Dichlorodihydrofluorescein diacetate (H2DCFDA, HY-D0940, MCE) was utilized to estimate the ROS levels via a previously described method.[86] Briefly, denuded mouse oocytes were incubated in HEPES-buffered KSOM (HKSOM) medium containing 5 μM H2DCFDA in the dark for 30 min at 37°C and then washed three times in HKSOM medium prior to being mounted on a glass slide and imaged with a fluorescence microscope. Mouse cumulus cells were incubated with 5 μM H2DCFDA solution in PBS in the dark for 30 min at 37°C, washed three times with PBS, and fluorescence was detected and imaged with an Axio-Imager Z2 fluorescence microscope (Carl Zeiss).

Immunofluorescence microscopy of mouse samples

In accordance with a previous method,[87] the spindles and chromatin of mouse oocytes were stained and observed via immunofluorescence microscopy. Mouse oocytes were fixed in fixative (MTSB XF) at 37°C for at least 30 min and then washed four times with washing buffer (phosphate-buffered saline supplemented with 0.02% NaN3, 0.01% Triton X-100, 0.2% nonfat dry milk, 2% goat serum, 2% bovine serum albumin and 0.1 M glycine). Afterward, the oocytes were left in washing buffer for 2 h at 37°C for blocking. Oocytes were incubated with FITC-α-tubulin (1:100, F2168, Sigma) overnight at 4°C. Next, the samples were washed and stained with DAPI to label the DNA.

For the expression of p-S6 and S6, fixed oocytes were left in washing buffer for 2 h at 37°C for blocking and then incubated with p-S6 (1:100, 4858S, Cell Signaling Technology) and S6 (1:100, 2217S, Cell Signaling Technology) antibodies overnight at 4°C. Oocytes were washed and incubated with secondary donkey anti-rabbit IgG Alexa Fluor 594 antibody (1:200, A-21207, Thermo Scientific) at 37°C for 2 h and stained with DAPI to label DNA. Oocytes were mounted on glass slides, sealed with nail polish, and imaged with an Axio-Imager Z2 fluorescence microscope (Carl Zeiss). ImageJ was used for relative fluorescence quantification.

Immunofluorescence microscopy of human samples

The cells were washed twice with PBS, fixed with fresh 3.7% paraformaldehyde for 30 min at 4°C, permeabilized with 0.1% Triton X-100 in blocking buffer (3% goat serum plus 0.1% BSA in PBS) for 20 min at room temperature (RT), incubated with blocking buffer for 1 h at RT, and stained with primary antibodies overnight at 4°C. The cells were subsequently incubated with fluorescence-labeled secondary antibodies for 2 h at RT. Hoechst 33342 (Thermo Scientific, H3570) was used to stain the nuclear DNA. The antibodies used in this experiment were as follows: H3K9me3 (1:200, ab8898, Abcam), H3K27me3 (1:200, 07–449, Millipore), LINE-1 ORF1p (1:100, MABC1152, Millipore), 53BP1 (1:300, ab36823, Abcam), donkey anti-rabbit IgG Alexa Fluor 594 (1:200, Thermo Scientific, A-21207), and donkey anti-mouse IgG Alexa Fluor 488 (1:200, Thermo Scientific, A-21202). The fluorescence was detected and imaged via an Axio-Imager Z2 fluorescence microscope (Carl Zeiss). The integrated fluorescence intensity was estimated via ImageJ software.

For LysoTracker red staining, the cells were seeded on glass bottom cell culture dishes (NEST, 801002, TC-treated). To stain the cells, 75 nM LysoTracker red (Beyotime, C1046) was added to the CC medium for 30 min at 37°C, and Hoechst 33342 was used to label the nuclear DNA. The cells were then washed once with CC medium, which was replaced with fresh CC medium, followed by confocal imaging. The lysosome inhibitor bafilomycin A (700 nM, Selleck, S1413) was added to CC medium for 6 h as a control.[88]

Proteostat staining was performed according to the instruction manual of the PROTEOSTAT Aggresome detection kit (Enzo Life Sciences; ENZ-51035-K25). Briefly, the cells were washed twice with PBS, fixed with 4% formaldehyde for 30 min at room temperature, treated with permeabilization solution (0.5% Triton X-100, 3 mM EDTA, pH 8.0) on ice, gently shaken for 30 min, washed twice with PBS, and stained with a 1:500 Proteostat in 1× Assay buffer for 2 h at room temperature and with Hoechst 33342 for nuclei. Afterward, the samples were washed twice with PBS and placed under coverslips on slides. The stained cells were imaged via confocal microscopy with a standard rhodamine filter set for cell aggresome signaling and a DAPI filter set for imaging the nuclear signal. The cells were treated with the proteasome inhibitor MG132 (10 μM, MCE, HY-13259) for 12 h as a control.[89]

For the LysoTracker and Proteostat staining experiments, we completed a total of five batches of independent experiments, and the same settings of confocal microscopy were applied to each batch of all experimental conditions. For the quantification of the LysoTracker$^+$ and Proteostat$^+$ areas per cell via ImageJ, the images were converted to black and white, and thresholds were set to outline the positive areas. The same threshold values were used for all images across all conditions in each batch of independent experiments.

For the proteostat staining of oocytes, refer to a previously published article.[66] Human GV oocytes were fixed with 4% formaldehyde for 1 h at room temperature and then washed and permeabilized with shaking on ice for 1 h. After brief washing, the oocytes were incubated with 1× assay buffer containing 0.1% BSA and a 1:500 Proteostat at room temperature. The oocytes were washed three times with 1×Assay Buffer containing 0.1% BSA, after which the fluorescence was imaged. Three batches of independent experiments were conducted.

Protein synthesis assay

Protein synthesis was performed according to the instructions of the BeyoClick HPG-594 Protein Synthesis Assay Kit (P1209S, Beyotime). Briefly, cumulus cells were incubated in 1× HPG working solution with methionine-free and serum-free culture medium for 30 min at 37°C, fixed at room temperature for 15 min, and permeabilized at room temperature for 15 min. Click reaction solution was prepared according to the instructions and incubated at room temperature in the dark for 30 min. Nuclear DNA was stained with Hoechst 33342 solution, and then fluorescence was imaged. Human cumulus cells were treated with rapamycin (0.50 μM) or CHX (0.30 μM) for three days.

AZT treatment

To inhibit L1 reverse transcriptase in cumulus cells, the collected cumulus cells were seeded into plates and then treated with 60 μM AZT (azidothymidine, Sigma–Aldrich, A2169) for 4 days. The administration and doses of AZT used in this study were based on

previous reports.[90] Moreover, we set up a series of concentration gradients and used immunofluorescence to further determine the appropriate concentration for detecting significantly reduced L1-ORF1 expression. After AZT treatment, cumulus cells were fixed and subjected to immunofluorescence and qRT–PCR.

Rapamycin and chaetocin treatment

The administration and doses of rapamycin were described in a previous article.[91] Rapamycin at 0.50 μM was added during IVM of the oocytes, and then, immunofluorescence and ROS detection were performed. Cumulus cells were seeded into plates and then treated with rapamycin (0.25 μM and 0.5 μM) for three days. Treating CCs with chaetocin (50 nM) for 24 h inhibited H3K9me3.[50]

Western blot

The cells were washed twice in PBS, lysed in cell lysis buffer on ice for 30 min and then sonicated for 1 min at an amplitude of 60 at 2 s intervals. After centrifugation at 10,000 × g for 10 min at 4°C, the supernatant was transferred into new tubes. The protein concentration of each sample was measured via bicinchoninic acid, and the protein samples were boiled in SDS sample buffer at 100°C for 10 min. The protein of each cell extract was resolved via 10% Acr-Bis SDS–PAGE and transferred to polyvinylidene difluoride (PVDF) membranes (Millipore). The membrane was blocked with 5% skim milk in TBST at room temperature for 2 h and then incubated with primary antibodies overnight at 4°C. β-actin served as a loading control. The immunoreactive bands were then probed for 2 h at RT with the appropriate horseradish peroxidase (HRP)-conjugated secondary antibodies. The protein bands were detected with a chemiluminescent HRP substrate (WBKLS0500, Millipore). The antibodies used for western blotting were as follows: *p*-mTOR (5536T, Cell Signaling Technology), mTOR (2983S, Cell Signaling Technology), p-S6 (4858S, Cell Signaling Technology), S6 (2217S, Cell Signaling Technology), p-4E-BP1 (9451T, Cell Signaling Technology), 4E-BP1 (9644T, Cell Signaling Technology), LC3 (14600-1-AP, Proteintech) and β-actin (AC026, ABclonal).

SA-β-gal staining

The senescence assay of cumulus cells was performed with a senescence-associated β-galactosidase staining kit (Beyotime, China, C0602) according to the manufacturer's instructions and a previous method.[92] Briefly, cumulus cells were washed three times with PBS and then fixed with 4% paraformaldehyde for 15 min at room temperature. After being washed three times with PBS, the cells were incubated overnight at 37°C in darkness with working solution containing 5-bromo-4-chloro-3-indolyl β-D-galactopyranoside (X-gal).

qRT–PCR

Detection of 18S and 28S abundance was conducted according to a previously published method.[38] Total RNA was extracted from cumulus cells via an RNeasy RNA Micro Kit (74034, QIAGEN) according to the manufacturer's instructions. Reverse transcription was performed on purified total RNA to generate cDNA via M-MLV reverse transcriptase (Invitrogen) and random hexamer primers (18S and 28S rRNAs) or Oligo (dT)18 primers according to the manufacturer's instructions. qPCR was performed with FastStart Universal SYBR Green Master Mix (4913914001, Roche) on an iCycler MyiQ2 detection system (Bio-Rad). Each sample was set up in duplicate and normalized to GAPDH. qPCR data were analyzed via the ΔΔCt method. qPCR primers (Table S7) were confirmed for their specificity via dissociation curves, and primer design for L1 was performed via a previously published method.[90]

RNA-seq library construction and sequencing

The isolation of gDNA and mRNA from individual cells was performed as previously described,[93] and separated mRNAs and gDNA were used for transcriptome analysis and other experiments (such as telomere length measurement), respectively. The RNA-seq library was constructed according to the Smart-seq2 protocol.[28] Briefly, single oocyte or CC samples were quickly placed in lysis buffer, and then reverse transcription, template switching and preamplification were performed to obtain cDNA. Next, RNA-Seq libraries were constructed with a TruePrep DNA Library Prep Kit V2 for Illumina (TD503-02, Vazyme Biotech) according to the instruction manual. The quality of the cDNA library was checked via qPCR analysis of the housekeeping gene *GAPDH*. For the accuracy and repeatability of the RNA-seq data, we performed a duplicate when we constructed a library for every single oocyte, and two samples of CCs (from the same donor as the oocytes) were collected for RNA-seq library construction. The final indexed libraries were pooled and sequenced on an Illumina HiSeq X10 platform with a 150-bp paired-end read length.

MethylC-seq library construction and sequencing

DNA methylation libraries of oocyte and CC samples were constructed according to a previously reported method with minor modifications.[94] For oocytes, 10 oocytes from 3 to 5 donors of similar age were collected in one tube as a sample. For cumulus cells, we collected CC samples from 6 donors of different ages and then performed DNA extraction in strict accordance with the instructions of the QIAamp DNA Micro Kit (56304, Qiagen). Detailed sample information, including age and sample size, is listed in Table S1.

Bisulfite conversion was performed on cell lysates with the following steps: incubation at 98°C for 10 min and 64°C for 120 min. DNA was eluted in 10 mM Tris-Cl (pH 8.5) and combined with 10 mM dNTPs, 5 μM BioPEA_N4_37 (5′-biotin-ACACTCTTTCCCTA CACGACGCTCTTCCGATCTNNN *N*-3′), and 10x NEBuffer 2 (E7645S, NEB, Ipswich, England) before incubation at 95°C for 5 min, followed by a 4°C pause for 2 min. Then, 75 U of Klenow Fragment (M0212M, NEB) was added, and the samples were

incubated at 4°C for 5 min, +1°C/15 s to 37°C, and 37°C for 30 min. Samples were incubated at 95°C for 1 min and transferred immediately to ice prior to the addition of fresh 1 mM dNTPs, 10 nM BioPEA_N4_37, 10x NEBuffer 2, and 75 U Klenow Fragment in a total volume of 2.75 μL. The samples were incubated at 4°C for 5 min and then at +1°C/15 s to 37°C for 30 min. This random priming and extension were repeated a further three times (five rounds in total). The samples were then incubated with 40 U of exonuclease I (M0293V, NEB) for 1 h at 37°C before the DNA was purified via 1× Agencourt Ampure XP beads (A63881, Beckman) according to the manufacturer's guidelines. The samples were eluted in 10 mM Tris-Cl (pH 8.5) and incubated with washed M-280 streptavidin Dynabeads (65001, Life Technologies) for 30 min with rotation at room temperature. The beads were washed twice with 0.1 N NaOH and twice with 10 mM Tris-Cl (pH 8.5), and resuspended in 48 μL reaction mixture: 10 mM dNTPs, 10x NEBuffer 2, and 10 μM Primer 2.0 (5′-GTGACTGGAGTTCAGACGTGTGCTCTTCCGATCTNNNN-3′). The samples were incubated at 95°C for 45 s and then transferred immediately to ice before the addition of 100 U of Klenow fragment and incubated at 4°C for 5 min, +1°C/15 s to 37°C, and 37°C for 90 min. Washed beads with 10 mM Tris-Cl (pH 8.5) and resuspended in 50 μL reaction mixture: 1 U of KAPA HiFi HotStart DNA Polymerase (KK2801, KAPA Biosystems), 10 μM Primer 1.0 (5′-AATGATACGGCGACCACCGAGATCTA CACTCTTTCCCTACACGACGCTCTTCCGATCT-3'), and 10 μM Index. Libraries were then amplified via PCR as follows: 98°C for 45 s; eight repeats of (98°C for 15 s; 65°C for 30 s; 72°C for 30 s); 72°C for 1 min; and a hold at 4°C. Amplified libraries were purified via 0.8 × Agencourt Ampure XP beads. The samples were eluted in another 27 μL reaction mixture: 1 U KAPA HiFi HotStart DNA Polymerase, 10 μM Primer 1.0 forward primer, and 10 μM Index, and amplified by PCR for an additional eight repeats. Amplified libraries were assessed for quality and quantity via high-sensitivity DNA chips on an Agilent Bioanalyzer. The DNA methylation libraries were sequenced by Annoroad via a HiSeq X10 platform with a 150-bp paired-end read length.

CUT&Tag

As described previously,[95] female CC samples were harvested and centrifuged for 3 min at 600 × g at RT. The cells were washed with 1 mL of wash buffer (20 mM HEPES pH 7.5, 150 mM NaCl, 0.5 mM spermidine, and 1 × protease inhibitor cocktail) by gentle pipetting and centrifuged for 3 min at 600 × g at RT. Concanavalin A-coated magnetic beads (Bangs Laboratories, BP531) were washed three times with binding buffer (20 mM HEPES pH 7.5, 10 mM KCl, 1 mM $MnCl_2$ and 1 mM $CaCl_2$) and then resuspended in the original volume of binding buffer. Ten microliters of activated beads were added per sample, incubated at RT for 10 min and collected with a magnet stand. The bead-bound cells and 2 μL of H3K9me3 antibody (Abcam, ab8898) were resuspended in 100 μL of antibody buffer containing 2 mM EDTA and 0.1% BSA in 2 mL of Dig-wash buffer (0.05% digitonin in Wash buffer) and rotated at RT for 2 h. The mixture was collected by a magnet stand, the supernatant was discarded, and the mixture was then incubated with a secondary antibody (1:100) diluted in Dig-wash buffer at RT for 1 h. The mixture was washed three times with Dig-wash buffer by using a magnet stand. The pG-Tn5 adaptor complex (~0.04 μM) was prepared in Dig-300 buffer (20 mM HEPES pH 7.5, 300 mM NaCl, 0.5 mM spermidine, 1 × protease inhibitor cocktail and 0.05% digitonin) at a 1:100 dilution, and 100 μL was added to the cells with the liquid removed and gently rotated at RT for 1 h. The mixture was collected by a magnet stand and washed three times in Dig-300 buffer. Next, the cells were resuspended in 300 μL of tagmentation buffer (10 mM $MgCl_2$ in Dig-300 buffer), and the mixture was gently mixed and incubated at 37°C for 1 h. To stop the reaction, 10 μL of 0.5 M EDTA, 3 μL of 10% SDS, and 2.5 μL of 20 mg/mL proteinase K were added to the sample, and the mixture was incubated at 37°C overnight. The fragmented DNA in the mixture was extracted via a standard phenol–chloroform extraction procedure.

To amplify the libraries, 24 μL of DNA was mixed with 5 μL of ddH2O, 10 μL of 5 × TAB (TD503-02, Vazyme Biotech), 1 μL of TAE (TD503-02, Vazyme Biotech), and 5 μL each of uniquely barcoded P5 and P7 primers (TD204-207, Vazyme Biotech), and each sample contained a different barcode. The amplification reaction was performed with the following cycling conditions: 72°C for 3 min; 98°C for 30 s; 15 cycles of 98°C for 15 s, 60°C for 30 s, and 72°C for 3 min; a final extension at 72°C for 5 min; and a hold at 4°C. Purified DNA libraries were tested for high quality prior to high-throughput sequencing. The libraries were sequenced on an Illumina NovaSeq 6000 platform with a 150-bp paired-end read length by Novogene.

We collected two batches of CC samples, and in each batch of experiments, the young and older samples were collected on the same day. However, owing to the limited number of samples, the number of cells in the two batches was not consistent (10,000 and 30,000 cells), but the number of cells in different age groups in the same batch was consistent (30 years versus 41 years & 31 years versus 39 years).

QUANTIFICATION AND STATISTICAL ANALYSIS

RNA-seq data processing

The raw RNA-seq data with low-quality bases and adapters were trimmed via Trimmomatic to obtain clean reads.[70] Next, the trimmed clean reads were aligned to the UCSC human hg19 reference genome via HISAT2 with the default settings.[71] featureCounts was further used to calculate read counts for each annotated gene using the -M parameter.[72] The gene expression level in a sample was quantified as the transcripts per million (TPM), which was calculated according to the following formula: $TPM_{ij} = \frac{C_{ij} \ / \ \text{length of gene } i}{\sum_i C_{ij} \ / \ \text{length of gene } i} \times 10^6$, where C_{ij} was the count value of gene i in sample j. For all sequenced cells, we counted the number of genes detected in each cell, and cells with fewer than 10,000 genes or 1,000,000 mapped reads were filtered out. After the critical filtering process, 48 sets of RNA-seq data from oocytes and 30 sets of RNA-seq data from CC samples were retained for downstream

analysis. To ensure the accuracy of the gene expression levels, only genes with TPM >1 in at least ten oocyte or CC samples were analyzed. The total mapped reads and mapped ratios are shown (Figures S1C–S1E) and the median number of genes detected was 16,105 in each oocyte or 21,255 in CC samples.

Identification of aging-specific genes and functional analysis

The read counts were loaded into RStudio (v4.1.0), and the critical filtering process was performed to filter out genes with low expression. Aging-specific genes were defined via correlation analysis. Next, we computed Pearson's correlations between donor age and the expression levels of genes (TPM) via 'cor' in R language and identified aging-specific genes via Pearson's coefficient (defined as the age coefficient). For oocytes, aging-specific genes were defined as those with an age coefficient threshold of 0.4 ($\geq$0.4, upregulated genes with age) or $-$0.4 ($\leq -$0.4, downregulated genes with age), after testing the significant differences of gene expression with age using various age-correlation coefficient cutoffs, based on the principle described.[29,30] For the CC samples, aging-specific genes were defined as those with an age coefficient threshold of 0.5 ($\geq$0.5, upregulated genes with age) or $-$0.5 ($\leq -$0.5, downregulated genes with age), after testing various cut-offs as above.

Gene Ontology (GO) and Kyoto Encyclopedia of Genes and Genomes (KEGG) analyses of aging-specific genes were performed via DAVID (v6.8),[73] and only enriched pathways whose p value was <0.05 were considered significantly enriched. The interactions between translation- and ribosome-related GO enrichments and related genes were generated via Cytoscape (v3.9.1).[74] GSEA was conducted to identify enrichments associated with aging in oocytes and cumulus cells, and only gene sets with an FDR <0.05 were considered significantly enriched.[75]

Transposable element analysis

For transposable element analysis, clean reads were aligned to the UCSC human hg19 reference genome by STAR with the parameters '-winAnchorMultimapNmax 100' and '-outFilterMultimapNmax 100'.[96] Referring to a previously published study,[97] only the TEs whose distributions in intergenic regions were mapped were considered, excluding the locations between the transcription start sites and transcription end sites of genes. TEs annotated via the UCSC Genome Browser (RepeatMasker) were counted via featureCounts. The median mapped rates were 11.8% for the oocytes and 16.8% for the CC samples, and the median mapped reads were 612,781 for the oocytes and 1,905,441 for the CC samples. TE expression was evaluated as counts per million (CPM). To ensure the accuracy of TE expression, only TEs with CPM >1 in at least ten oocytes and CPM >2 in at least ten CC samples were analyzed.

Identification of aging-specific TEs

After critical filtering to remove TEs with low expression, aging-specific TEs were identified via correlation analysis. Specifically, Pearson's correlations between donor age and the expression levels of TEs (CPMs) were computed via 'cor' in R language, and then, aging-specific TEs were determined via Pearson's coefficient (defined as the age coefficient) with a threshold of 0.4. Age coefficients $\geq$0.4 were defined as TEs whose expression increased with age, whereas those $\leq -$0.4 were defined as TEs whose expression decreased with age.

MethylC-seq data processing

Adaptors and low-quality bases of bisulfite sequencing reads were first trimmed by Trimmomatic (http://www.usadellab.org/cms/index.php?page=trimmomatic) with default parameters. Next, reads that passed quality control were mapped to the human reference genome (hg19) via Bismark (version 0.19.1)[76] in paired-end alignment mode. Only reads with a unique mapping location in the genome were retained for further analysis. After alignment, the reads were further deduplicated via Picard (http://broadinstitute.github.io/picard/). The bisulfite conversion rate was estimated by the spike-in of unmethylated lambda DNA. Methylation calls were extracted via the Bismark methylation extractor.

The annotations of exons, introns, CGIs, TSSs and transcription end sites (TESs) were downloaded from the UCSC Genome Browser (hg19). All repetitive element annotations were downloaded from RepeatMasker (hg19) via the UCSC Genome Browser. Promoter regions were defined as the 1 kb upstream to 1 kb downstream of transcription start sites (TSSs).[98]

The methylation levels of the CpGs were quantified according to previously published methods.[99] For each CpG, the DNA methylation level was determined by the ratio of the number of reads supporting C (methylated) to the total number of reads (methylated and unmethylated).

Metaplots of CpG methylation levels were generated by calculating the degree of methylation within each RefSeq gene and ten 1 kb windows of flanking sequences.

MethylC-seq data analysis

Initially, the human genome was divided into 1 kb tiles, and tiles with at least 3 CpGs covered by both age groups in a comparison were considered the background to find DMRs. For tiles that passed the criteria, the methylation level of each retained tile was determined as the ratio of the number of alignments with C (methylated) to the sum of the alignments with C and T for all the CpGs in the tile. When identifying DMRs in oocyte or CC samples of different age groups, we used the calculateDiffMeth function from the methylKit R package with the following criteria: difference in methylation >20% and adjusted p value <0.05, which were adjusted via the SLIM method.[77,98,100]

Hierarchical clustering via Euclidean distance metrics derived from methylation levels per DMR for each age group was conducted via the clusterSamples function from the methylKit R package with the 'ward' agglomeration method.

The distance of DMRs from the TSS was calculated on the basis of a previously published method.[101] Briefly, the distance was reported by subtracting the mean DMR genomic localization from the TSS positions, grouping the distances into 500-bp clusters from position −10 kb to position +10 kb, and quantifying the DMRs in each cluster. DMRs with a distance of more than 10 kb from the respective TSS were excluded and not counted.

Enrichment analysis of genes with differentially methylated regions was performed via DAVID 6.8 (https://david.ncifcrf.gov). Enriched pathways with a p value less than 0.05 were considered statistically significant. The differentially methylated regions used for enrichment analysis contained only gene bodies, promoters and CGIs, and regions located on intergenic and transposable elements were excluded.

Integrated analysis of DNA methylation and the transcriptome

To correlate the epigenetic and transcriptome datasets, DMRs were annotated to the nearest transcription start site via the annotatePeaks.pl function in HOMER (v4.11.1).[102] Only DMRs located in the gene body, promoter, and CGI regions were used for association analysis. DESeq2[78] was used to obtain the statistical significance of the DEGs of different groups, and only the genes with a fold change greater than 1.2 and adjusted p value <0.05 from the DEseq2 results were considered to be differentially expressed. Adjusted p values were computed in DESeq2 via the Wald test and adjusted for multiple testing via the procedure of Benjamini and Hochberg.[103]

CUT&Tag processing and analysis

The raw data were processed according to the following pipeline. The sequencing adapters were trimmed, and read pairs with low quality or low complexity were filtered from the raw data through TrimGalore (v0.5.0). The trimmed read pairs were aligned to the human reference genome hg19 via Bowtie2 (v2.3.4)[79] with default parameters. For peak calling, the parameters used were macs2 callpeak ''-q 0.05 -g hs –keep-dup all''.[80,95] For annotation and enrichment analysis of the genomic regions, we referred to previously published methods.[104] First, the ''annotatePeak'' function in the R package ChIPseeker (v1.28.3)[81] was utilized to profile the distribution of genomic regions. Second, the functional enrichment of genes that are marked by or near H3K9me3 peaks was analyzed via Genomic Regions Enrichment of Annotations Tool (GREAT) analysis with default settings via the R package rGREAT (v1.24.0).[105] We used the 'macs2 bdgdiff' function to identify young-specific and old-specific H3K9me3 peaks. We utilized the ''intersect'' subcommand in bedtools (v2.27.1) to identify peaks related to ribosome- and lysosome-related genes, including promoters and gene bodies, and these ribosome- and lysosome-related genes were defined via RNA-seq data via correlation analysis. For data visualization, bigwig files were generated via bamCoverage and merged via bigWigMerge, and H3K9me3 modification signals around peaks were visualized via deepTools (v3.2.0).[82] Promoters were defined as the regions 1 kb upstream and 1 kb downstream of TSSs. Gene bodies were defined as the regions from the TSSs to the TESs.

Statistical analysis

Statistical analyses were performed via an unpaired two-tailed Student's t test in PRISM software (GraphPad 8 Software) to compare the differences between the treatment and control groups, assuming equal variance. The Mann–Whitney test was used to determine the significance of differences between data without a normal distribution. One-way or two-way ANOVA with Tukey's test was used for multiple comparisons. The chi-square test was used to test differences between two groups for categorical variables. *, **, *** and **** indicate $p < 0.05$, $p < 0.01$, $p < 0.001$ and $p < 0.0001$, respectively. NS indicates not significant. The bioinformatics data were statistically analyzed via a two-tailed t test with R software, and p values are indicated in each figure. Correlations between clinical indicators and age and the corresponding statistical significance were calculated on the basis of Pearson's rank correlation coefficient (r).

For correlation analysis between the age and gene expression levels, p values were adjusted using the Benjamini–Hochberg (BH) method. Selection criteria for age-correlation coefficient cut-offs included, (1) statistically significant correlations (BH-adjusted $p < 0.05$), and (2) at least moderate correlation between age and gene expression levels ($|r| \geq 0.4$).[29,30]

For the clinical trials of rapamycin therapy, categorical data are presented as frequencies and percentages, and between-group comparisons were conducted with the chi-square test. Continuous data are expressed as the means (±SD) or medians (Q1, Q3), with a Wilcoxon rank-sum test for between-group differences. The detailed clinical information of the control group and the rapamycin group is presented in Tables S5 and S6.

ADDITIONAL RESOURCES

The study has been registered on the Chinese Clinical Trial Registry (https://www.chictr.org.cn/) with registration number (ChiCTR2300069828).